

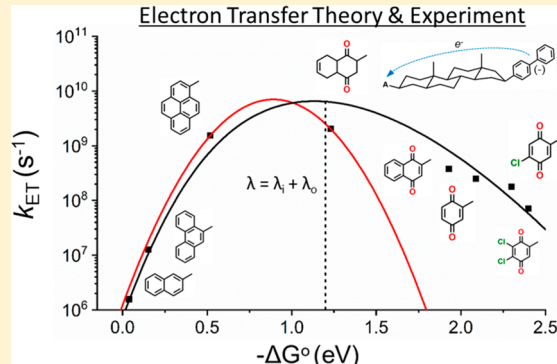
Introduction to Electron Transfer: Theoretical Foundations and Pedagogical Examples

Eric J. Piechota¹ and Gerald J. Meyer^{*1,2}

Department of Chemistry, University of North Carolina at Chapel Hill, Chapel Hill, North Carolina 27599, United States

ABSTRACT: A central theme in introductory and advanced chemical education courses pertains directly to the transfer of electrons between atoms, ions, or molecules. This article presents theoretical treatments of electron transfer with specific attention toward applying these principles to experiment. The goal is to revitalize teaching electron transfer at the undergraduate and graduate levels. Central theoretical aspects are presented through the construction of Gibbs free (potential) energy surfaces with definitions and semiquantitative descriptions of the three key parameters necessary to compute electron transfer rate constants with Marcus theory: (1) the Gibbs free energy change, ΔG° ; (2) the reorganization energy, λ ; and (3) the electronic coupling between D and A wave functions, H_{DA} . A simplified description of this theory is presented with classical free energy surfaces for the electron donor and acceptor wherein the force constant in Hooke's Law is replaced by λ . Variation of ΔG° results in a Gaussian distribution of activation energies that give rise to Marcus normal, activationless, and inverted kinetic behaviors. Classical and contemporary experimental examples that have tested and utilized Marcus theory are described, including the first validation of the inverted kinetic region. It is shown that, as the donor–acceptor coupling increases, adiabatic electron transfer may result where it becomes more difficult to decouple the Marcus parameters through experiment. The trials and tribulations of doing so are described that provide context and enable readers to understand the prior electron transfer literature and use the pedagogical foundations presented herein for their own learning and pleasure.

KEYWORDS: History/Philosophy, Textbooks/Reference Books, Oxidation/Reduction, Electron Transfer, Equilibrium, Kinetics, Mechanisms of Reactions, Theoretical Chemistry



Electrons are of central importance to chemical transformations and are justifiably emphasized in all levels of chemistry education. Many reports in this *Journal* emphasize the role of electrons in general chemistry through Lewis structures^{1,2} that show electrons can be paired, shared, and transferred in reduction/oxidation (redox) reactions.^{3,4} Moreover, reaction mechanisms in organic chemistry highlight the importance of orbital overlap and electron densities in bond-forming transformations.^{5,6} Inorganic textbooks often detail Taube's compelling evidence for an *inner-sphere* mechanism, where an ion or molecule bridges the donor and acceptor during electron transfer. In contrast, an *outer-sphere* mechanism is understood to occur when the coordination spheres are maintained throughout the reaction.⁷ Physical chemistry underscores the importance of discrete electronic energy levels in atomic and molecular spectra⁸ and excited-state electron transfer reactions.^{9,10} Finally, biochemistry offers examples of vectorial electron transfer along spatially arranged redox active species whose reduction potentials provide an energy gradient for transport over long distances.^{11–15} Central in this regard are the theoretical models which are the foundation for understanding the kinetics and mechanisms of electron transfer.¹⁶

This article first describes the connection between chemical equilibria and kinetics for electron transfer reactions. It then presents the underlying expectations that formulate the practical model through which these reactions are understood and applies it to experimental examples. Special emphasis is added to bridge the gap between mechanistic extremes of nonadiabatic and adiabatic electron transfer as the underlying theory differs.^{17,18} Indeed, to students and researchers alike some difficulty may arise when deciding which regime a reaction belongs to or if it has intermediate behavior. It is often unclear why authors of previously published studies selected one extreme over the other. Adding to the confusion is the fact that an *inner-sphere* electron transfer mechanism does not necessarily indicate an adiabatic electronic transfer reaction. Likewise, an *outer-sphere* electron transfer reaction is not necessarily nonadiabatic.¹⁹ A additional goal of this article is to provide descriptions that enable one to interpret, or reinterpret, prior literature and to address new electron transfer results with appropriate theoretical models in order

Received: May 24, 2019

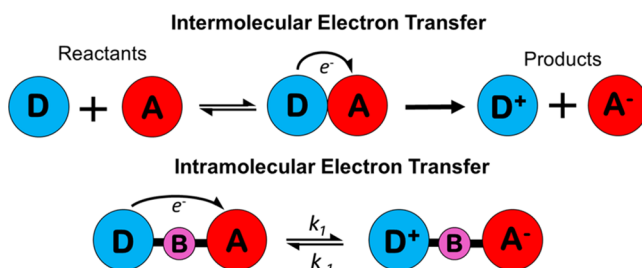
Revised: September 23, 2019

Published: October 28, 2019

to revitalize teaching electron transfer for researchers and students at all levels.

A convenient place to begin pedagogical discussions is with redox equilibrium as shown in **Scheme 1**.

Scheme 1. Intermolecular (Top)^a and Intramolecular (Bottom)^b Electron Transfer Reactions



^aThe donor and acceptor must diffuse together to form an “encounter complex” before electron transfer to form D^+ and A^- occurs.

^bInclusion of a rigid molecular bridge removes the need for diffusion and electron transfer instead occurs at a fixed geometric distance. In both cases, the electron transfer rate is controlled by the free energy change, ΔG° ; reorganization energy, λ ; and electronic coupling, H_{DA} .

Equilibrium as a “balance” oftentimes invokes the false perception that reverse reactions stop altogether under equilibrium conditions.²⁰ Instead, concentrations are time invariant due to a *dynamic* equilibrium where the opposing forces are rate constants whose values can be large and depend only on temperature.²¹ Forward (k_1) and reverse (k_{-1}) rate constants provide a direct measure of the equilibrium constant, $K_{eq} = k_1/k_{-1}$, and hence the free energy change, ΔG° , that enables students to accurately compute concentrations during redox titrations or the direction of current flow in galvanic cells. This establishes a realization that thermodynamics and kinetics for electron transfer are inherently linked. Formal reduction potentials, eq 1, afford an independent measure of K_{eq} through ΔG° and Faraday’s constant, F , although this fundamental relation is only precise when the electronic interactions at the instant of electron transfer are small and the reaction is nonadiabatic.

$$\begin{aligned}\Delta G^\circ &= -RT \ln(K_{eq}) = -F\Delta E^\circ \\ &= -nF[E^\circ(D^{+/0}) - E^\circ(A^{0/-})]\end{aligned}\quad (1)$$

This article describes donor–bridge–acceptor ($D-B-A$) compounds, where the bridge serves to mediate orbital overlap, and bimolecular electron transfer that occurs within a $[D, A]$ encounter complex, Scheme 1. A previously described composite mechanism enables a unimolecular electron transfer rate constant (s^{-1}) to be extracted from a measured bimolecular rate constant ($M^{-1} s^{-1}$).^{22–24} Electron transfer within the encounter complex and at fixed geometric distance is inherently unimolecular with rate constant units of s^{-1} .²⁵

With a clear connection between kinetics and thermodynamics for electron transfer reactions established, defining the theoretical framework becomes important. This is accomplished beginning with the construction of potential energy surfaces and by defining critical Marcus parameters and Franck–Condon factors that are expected govern electron transfer in homogenous solution.²⁶ This section is followed by a discussion of literature examples that apply the constructed models to real data and place them into a broader context.

FUNDAMENTAL ELECTRON TRANSFER THEORY

Marcus theory is the basis through which electron transfer chemistry and reactivity are understood.^{27–30} It enables the electron transfer rate constant, k_{ET} , to be calculated though the canonical high-temperature semiclassical expression, eq 2.³¹

$$k_{ET} = \frac{2\pi}{\hbar} \frac{H_{DA}^2}{\sqrt{4\pi\lambda k_b T}} \exp\left(-\frac{(\Delta G^\circ + \lambda)^2}{4\lambda k_b T}\right) \quad (2)$$

A remarkable aspect of this expression is that it permits electron transfer rate constants to be calculated as a function of only three variables that can be computed or determined experimentally, albeit not independently. The first Marcus parameter is the Gibbs free energy change, ΔG° , equivalently referred to as the driving force, $-\Delta G^\circ$, for the reaction is included in the exponential Franck–Condon weighted density of states to describe nuclear factors. Such vibrational or nuclear factors become important for *inverted* electron transfer reactions or at low temperatures where $\hbar\omega > k_b T$.

Other Marcus parameters are the reorganization energy, λ , and the electronic coupling, or degree of quantum mechanical mixing, between D and A wave functions, H_{DA} . Electronic coupling describes the energy stabilization gained from the interaction of D and A wave functions. The regime in which H_{DA} is small is commonly referred to as *nonadiabatic* electron transfer. By contrast, *adiabatic* electron transfer can occur when the electronic coupling is sufficiently large. This semiclassical expression has been shown to be valid for nonadiabatic or weakly adiabatic electron transfer.

It is here that many questions arise naturally: (1) What is the interplay between and influence of ΔG° , λ , and H_{DA} on the electron transfer rate? (2) How are nonadiabatic and adiabatic reactions different, and what are the limits of existing theories? (3) How do kinetics and spectra reflect and distinguish between (non)adiabatic regimes of electron transfer?

To answers these questions, a solid foundation in perhaps the most common research and pedagogical tool for visualizing electron transfer reactions is needed: potential energy surfaces (provided herein as Gibbs free energy) for the reactants and products. Reactant (or product) surfaces when thought of individually are not necessarily reflective of Marcus parameters. However, by defining a reactant and product surface, a so-called “reaction surface” can be constructed that is a function of all three Marcus parameters and provides a molecular-scale view of electron transfer.^{32,33}

Free Energy Surfaces

The complicated and sophisticated reality of electron transfer is generally simplified with two free energy surfaces, one that represents, for example, the $D-B-A$ reactants and one representing the D^+-B-A^- products.³⁴ These surfaces are functions of a nuclear configuration which signifies the spatial arrangement of solvent molecules as well as $D-B-A$ molecules with respect to equilibrium configurations.³⁵ The initial focus here is on weakly interacting redox centers that undergo *nonadiabatic* electron transfer. In this regime, motion along the reaction coordinate requires an electron “hop” from the reactant to product surface when the energies are equal. Reactions in this regime are constrained by the Born–Oppenheimer approximation that the motion of the electron is faster than translational, rotational, and vibrational nuclear motion.³⁶

In reality, there are $3N - 6$ dimensional vibrational degrees of freedom for D–B–A molecules and external solvent, where N is the number of atoms in the solvent or the D–B–A molecule comprising a multidimensional energy surface.^{37,38} A hallmark of Marcus theory is the simplification of nuclear degrees of freedom and changes in solvent polarization to be described by a collective harmonic vibrational coordinate with fixed force constants for reactants and products.³⁹ The force constants relate directly to the total *reorganization energy*, λ , for collective reactant/solvent motion occurring during the electron transfer reaction.³⁵ The resulting surfaces are interpreted as increases in energy following bond-length distortions and solvent polarization changes away from an equilibrium position.

$$G_R = \frac{1}{2}fX^2 = \lambda X^2 \quad (3)$$

$$G_p = \frac{1}{2}f(X - 1)^2 + \Delta G^\circ = \lambda(X - 1)^2 + \Delta G^\circ \quad (4)$$

Here, G_R and G_p are free energies for reactants and products, respectively, f is the force constant, X is the position along the reaction coordinate or nuclear configuration, and ΔG° is the driving force for the reaction. Hence, vertex coordinates for the reactants and product energies are offset by ΔG° ; the driving force for the reaction is reflected by the position of the product surface minima.

These two independent harmonic oscillator approximations allow the free energy of the reactant and product surfaces to be evaluated as a function of the nuclear configuration, X . An example for a self-exchange reaction where the donor and acceptor reactants and products differ by only one electron and $\Delta G^\circ = 0$ is given in Figure 1A. Note that a crossing point exists which corresponds to the activation free energy ΔG^\ddagger from transition-state theory.

Reorganization Energy

For Gibbs free energy surfaces the reorganization energy, λ , is defined as the difference in energy between the product surface and the reactant surface while both are in the equilibrium configuration of the reactants. Consider, for example, instantaneous light-induced electron transfer from D–B–A to form D⁺–B–A[−] in Scheme 1 and Figure 1B. An electron was transferred from D to A, yet progress along the reaction coordinate did not occur (a manifestation of the Born–Oppenheimer approximation). Electron transfer altered the charge density distribution of the molecule without nuclear motion. This results in the formation of a higher-energy state as outer-sphere solvent motion and inner-sphere D–B–A bond length and angle rearrangements to stabilize the new charge distribution do not occur during electron transfer. In other words, outer-and inner-sphere *reorganization* has not occurred in order to accommodate the new product equilibrium nuclear configuration.

Thermal electron transfer results when the reactant and product energies are degenerate, Figure 1B, and occurs at the crossing point between the reactant and product surfaces, with an activation energy that is 1/4 that of the reorganization energy, $\Delta G^\ddagger = \lambda/4$ for a self-exchange reaction. For nonadiabatic reactions, the motion of solvent molecules and intramolecular vibrations are often coupled yet remain independent of electronic motion in accordance with the Born–Oppenheimer approximation. Partial reorganization is necessary in order for a D–B–A reactant to achieve the

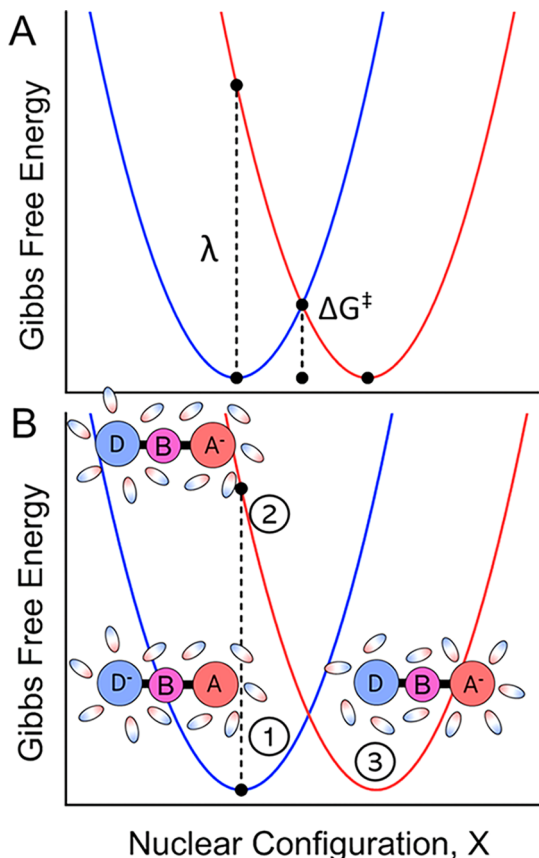


Figure 1. (A) Isoenergetic Gibbs free energy surfaces calculated from eqs 3 and 4. Surfaces correspond to an electron transfer reaction from the equilibrium configuration of the D–B–A reactants (blue parabola) through the transition state, ΔG^\ddagger , to the D⁺–B–A[−] products (red parabola). The reorganization energy, λ , is shown as the energy difference between the product and reactant surfaces. (B) A molecular view of the reorganization energy corresponding to thermal and optical nonadiabatic electron transfer when $\Delta G^\circ \approx 0$. (1) → (2), Optical: Beginning from the equilibrium configuration of the reactants and surrounding solvent molecules, absorption of light with $E = h\nu = \lambda$ generates the electronic configuration of the product, D⁺–B–A[−], at a fixed nuclear position. Higher energy is a result of fixed orientation of solvent dipoles relative to the ground state. (1) → (3), Thermal: From the equilibrium configuration of the reactants, electron transfer occurs instantaneously when the product and reactant energies are degenerate at the transition state, $\Delta G^\ddagger = \lambda/4$. Formation of the equilibrium electronic and nuclear configuration of the product occurs as a solvent molecule relaxes to stabilize the new electronic configuration.

necessary transition-state energy, the probability of which is Boltzmann averaged, $\Delta G^\ddagger/k_b T$. Because changes in the nuclear configuration have already occurred, the transition-state energy is lower. After reaching the transition state, electron transfer occurs from the reactant to the product surface with subsequent motion of solvent and internal vibrational modes that stabilize the D⁺–B–A[−] reaction product.

The reorganization energies correspond to the free energy stored in a destabilized solvent environment around D⁺–B–A[−] plus the nonequilibrium bond lengths and vibrational frequencies that are sensitive to electron density. It follows that both “outer-sphere” (λ_o) and “inner-sphere” (λ_i) components contribute to the total reorganization energy, $\lambda = \lambda_i + \lambda_o$.⁴⁰ Insight into the individual contributions to the

reorganization energy requires revisiting the initial definition of the potential energy surfaces.

In the case of inner-sphere components to the reorganization energy, an increase in energy is expected for bond-length displacement away from the equilibrium position as described by Hooke's law. For a particular bond, j , with a force constant, f_j , the corresponding square of the change in bond length is the dominant contributor to λ_i given by eq 5.

$$\lambda_i = n \left[\frac{1}{2} \sum_j f_j (d_p - d_r)^2 \right] \quad (5)$$

Here, d_p and d_r are the product and reactant equilibrium bond lengths, and n is the number of bonds involved in the reaction. Equation 5 predicts a large λ_i when significant bond-length changes accompany electron transfer.

Outer-sphere contributions to the reorganization energy correspond to the response of the solvent dielectric to the new electronic density distribution. The solvent optical, ϵ_{op} , and static, ϵ_s , dielectric constants as well as the geometric D–A distance, R , and the radii of the donor, r_D , and acceptor, r_A , all influence λ_o in dielectric continuum theory, eq 6.^{27,41}

$$\lambda_o = \frac{e^2}{4\pi\epsilon_0} \left(\frac{1}{2r_D} - \frac{1}{2r_A} + \frac{1}{R} \left(\frac{1}{\epsilon_{op}} - \frac{1}{\epsilon_s} \right) \right) \quad (6)$$

In intramolecular electron transfer reactions, R is often much larger than the sum of the donor and acceptor radii because the covalent bridge fixes the positions of the reacting species. Surprisingly, structural changes associated with electron transfer are often minimal such that $\lambda = \lambda_i + \lambda_o \approx \lambda_o$, and outer-sphere contributions are dominant. Exceptions to this expectation exist in redox reactions that involve significant Jahn–Teller or other molecular distortions to reach the transition state.

Gibbs Free Energy and Activation Energy

When eqs 3 and 4 are set equal and used to determine the energy at which the curves intersect, eq 7 results which relate the barrier to the driving force, ΔG° , and reorganization energy.

$$\Delta G^\ddagger = \frac{(\Delta G^\circ + \lambda)^2}{4\lambda} \quad (7)$$

This expression provides a rare and explicit connection between chemical kinetics and reaction thermodynamics⁴² with a predicted parabolic dependence of ΔG^\ddagger on ΔG° that gives rise to three kinetic regimes for electron transfer: (1) normal, $-\Delta G^\circ < \lambda$; (2) activationless, $-\Delta G^\circ = \lambda$; and (3) inverted, $-\Delta G^\circ > \lambda$. In other words, with increased driving force, $-\Delta G^\circ$, the barrier will decrease, become zero, and then subsequently increase as is shown in Figure 2. Hence, a counterintuitive yet profound prediction of Marcus theory is that very exergonic reactions slow down relative to lower driving forces and a maximum rate constant is achieved when the reaction becomes *barrierless*, at $-\Delta G^\circ = \lambda$ when $\Delta G^\ddagger = 0$.

Electronic Coupling

Molecular orbitals facilitate electron delocalization and D–A wave function mixing prior to electron transfer. Delocalization is expected to fundamentally alter the potential energy surfaces, causing individual chemical identities and properties of the redox centers to become intertwined. Behavior indicative of

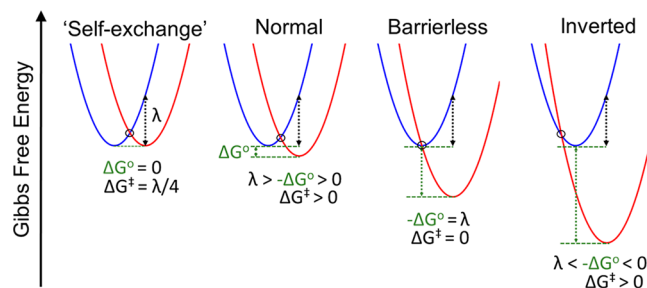


Figure 2. Types of electron transfer reactions as defined by the reaction free energy, ΔG° , and reorganization energy, λ . (From left to right) Self-exchange reactions between energetically degenerate donors and acceptors. “Normal” electron transfer reactions, $\lambda > -\Delta G^\circ > 0$. “Barrierless” reactions when $\lambda = \Delta G^\circ$, which corresponds to a rate maximum. “Inverted” electron transfer when $\lambda < -\Delta G^\circ$ which is predicted to result in a decrease in rate of electron transfer. Note that λ is constant across the series.

electronic interaction is often associated with new spectroscopic features, altered reduction potentials, or even expected from molecular structures.^{35,43} This phenomenon is referred to as electronic coupling, H_{DA} .

A prediction of quantum mechanics is that wave function amplitudes decay exponentially with distance providing finite overlap, even across long distances. Such coupling can facilitate long distance nonadiabatic electron transfer, Figure 3A. An

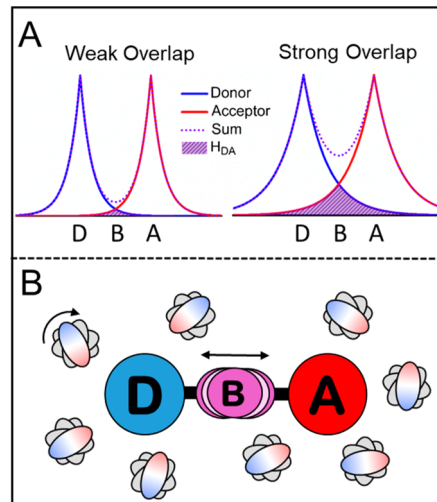


Figure 3. (A) Descriptive orbital overlap that leads to electronic coupling, H_{DA} , between a molecular donor and acceptor. Wave function amplitudes decay exponentially, and when a molecular bridge does not facilitate overlap, electronic coupling is weak, yet remains nonzero (left). When bridge orbitals facilitate D–A overlap, electronic coupling increases and overlap can be considerable. Mixing facilitated by a molecular bridge begins to impact the free energy surfaces. (B) When free energy surfaces are sufficiently impacted by H_{DA} , electron motion becomes coupled to the nuclear configuration. Thus, the rate of electron transfer is influenced by inner-sphere (vibrational) and outer-sphere (solvent rotational) motion.

exponential decay of electronic coupling as the donor and acceptor wave function separation is captured through an attenuation factor, β , which serves as a constant that may be diagnostic of the electron transfer mechanism. Electronic coupling when the donor/acceptor are at van der Waals separation, R_o , is given by H_{DA}^o eq 8.^{44,45}

$$H_{DA} = H_{DA}^o \exp\left(-\frac{\beta}{2}(R_{DA} - R_o)\right) \quad (8)$$

Together, eq 8 and eq 2 can be used to predict distance-dependent electron transfer rate constants, eq 9.

$$k_{ET} = k_{ET}^o \exp(-\beta(R_{DA} - R_o)) \quad (9)$$

Robin and Day⁴⁶ classified three regimes of electron delocalization based on the magnitude of the electronic coupling between the donor and acceptor, Figure 4.⁴⁷ When $H_{DA} = 0$, electron density is formally localized on the noninteracting donor or acceptor site and is defined as a Class I compound.

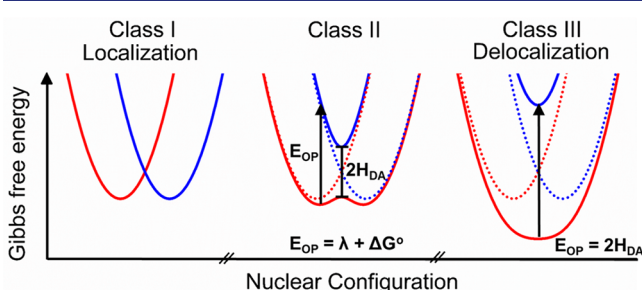
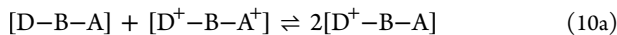


Figure 4. Effect of electronic coupling on potential energy surfaces as categorized by Robin and Day. Class I electron transfer (top left) corresponds to $H_{DA} = 0$; electrons are valence-localized, with a maximum barrier for electron transfer ΔG^\ddagger . In class II, $H_{DA} > 0$, electron density is partially delocalized (top middle), yet electron transfer between reactants and products is discrete (and can be adiabatic), while the barrier is reduced $\Delta G_{ad}^\ddagger < \Delta G^\ddagger$. In class III, electron density is delocalized (right), and electron transfer occurs between delocalized electronic states; there is no barrier for thermal electron transfer, $\Delta G^\ddagger = 0$.

Much more relevant, and of experimental interest, are intermittent values of $0 < H_{DA} < \lambda/2$ which are known as Class II compounds. In this case, the interaction between reactant and donor wave functions, mediated through electronic coupling, results in the generation of a new ground- and excited-state surface. Hence, this changes the individual noninteracting surfaces into two new mixed states. In fact, when $H_{DA} > 0$, redox and spectroscopic properties of the individual donor and acceptor become mixed, oftentimes giving rise to unexpected changes in formal reduction potentials that influence the comproportionation reaction that often has a favorable equilibrium constant, $K_c \gg 0$, as defined in eqs 10a and 10b.^{48–50}



$$K_c = \frac{[D^+BA]^2}{[DBA][D^+BA^+]} \quad (10b)$$

Mixing between a donor and acceptor may also be evident by the appearance of optical intervalence charge transfer (IVCT) transitions in the visible and infrared spectroscopic regions, that occur at an energy $E_{op} = \lambda + \Delta G^\circ$. A classical IVCT example is given in Figure 10 and is discussed further for Class III compounds. More crucial, however, for Class II, is that discrete minima still exist, the free energy barrier for thermal electron transfer is not zero, and an electron transfer

equilibrium exists between the D–B–A and D^+-B-A^- surfaces.

For Class III compounds electronic coupling is sufficiently large such that individual molecular properties are averaged, electron density is completely delocalized between the D and A (provided $\Delta G^\circ = 0$), and a redox equilibrium is no longer strictly defined.⁴⁷ In symmetric compounds discrete thermal electron transfer does not occur, yet IVCT transitions between the ground and excited states are well-known,^{51–53} where the optical absorption occurs at $E_{op} = 2H_{DA}$ because the donor and acceptor electron densities are averaged.⁵⁴ As a result, optical transitions of Class III molecules are often asymmetric as photons with energies less than $2H_{DA}$ are not absorbed. This leads to the observation of asymmetric, or skewed, Gaussian bands.

For class I or II electron transfer that exhibits Gaussian-shaped IVCT bands, the corresponding intensities (extinction coefficient, ϵ_{max}), transition widths (full-widths at half-maximum intensity, $\Delta\nu_{1/2}$), and donor–acceptor geometric distances are used to calculate the extent of coupling, H_{DA} , through Mulliken–Hush analysis, eq 11.^{54,55}

$$H_{DA} = \frac{0.0206}{r} (E_{op} \epsilon_{max} \Delta\nu_{1/2}) \quad (11)$$

Geometric estimates of the charge transfer distance generally provide a lower limit of H_{DA} as wave function delocalization results in a decreased electron transfer distance.^{56–58}

The impact of electronic coupling on free energy surfaces provides a distinction between nonadiabatic and adiabatic electron transfer:⁵⁹ nonadiabatic transfer requires an instantaneous “hop” from the reactant to product surface at the transition state with a corresponding probability (e.g., transmission coefficient) less than 1, while adiabatic electron transfer allows for continuous motion along the nuclear configuration with a near unity transmission coefficient. Such contrasting features of adiabatic and nonadiabatic electron transfer are shown in Figure 5.^{60,61} Hence, as H_{DA} decreases, so does the probability for electron transfer between the reactant to product surfaces to occur. Even if the nuclear configuration of the products and reactants is in the optimal transition-state configuration, the reaction may not occur and the nuclear configuration instead remains on the reactant surface.⁶² In this regime, the electron transfer rate constant is proportional to the square of the electronic coupling as in eq 2.⁶³

As the electronic coupling increases, the probability of passing through the transition state also increases up to a maximum of 1. At this crucial point, the mechanism of electron transfer fundamentally changes, Figure 3B.^{64,65} This provides one definition of adiabatic electron transfer: the transmission coefficient from the reactant to the product surface is unity, $\kappa = 1$.⁶⁶ However, the magnitude of H_{DA} necessary for the reaction to proceed adiabatically depends critically on the relative time scales of electron and nuclear motion.^{18,64,67}

Previously, the nonadiabatic Marcus expression, eq 2, was used to describe the electron transfer rate constant. However, the Robin–Day classification system shows that electronic coupling can alter the potential energy surfaces. Generally, it is nontrivial to determine whether a reaction is adiabatic or nonadiabatic. In principle, it is possible to quantitatively interpolate between nonadiabatic and adiabatic electron transfer mechanisms using the transmission coefficient alluded to above. The approach is commonly referred to as the Landau–Zener formalism^{68–70} that provides a ratio of

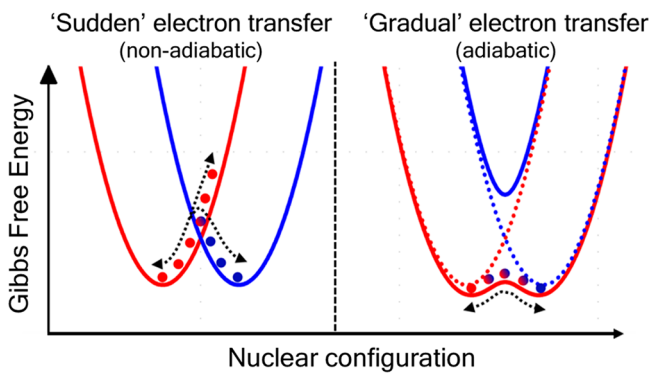


Figure 5. Nonadiabatic and adiabatic electron transfer reactions represented by static Gibbs free energy surfaces. (Left) Nonadiabatic electron transfer is characterized by weak electronic coupling and electronic factors in the transition state. When H_{DA} is small, the probability of a successful reaction is small, and electron transfer may not occur (dashed line on the reactant surface). However, because wave function overlap is finite, there is always nonzero probability that the reaction succeeds to form the product (dashed line crossing the transition state). (Right) Adiabatic electron transfer occurs when the coupling is sufficiently strong, with influences from nuclear motion, and the probability of a successful reaction approaches unity. In this case electron transfer occurs along the same low-energy surface (dashed line going interchangeably from reactants to products), occurring gradually. In this regime, electronic motion becomes coupled to nuclear motion of inner- and outer-sphere modes.

probabilities, P , for a transition from an initial to final state as a function of the electronic (ν_{el}) and nuclear frequencies (ν_n). The Landau–Zener expression for a reaction in the Marcus normal region is given by eq 12.^{71,72}

$$\kappa = \frac{2P}{1+P} = \frac{2\left(1 - \exp\left(-\frac{\nu_{el}}{2\nu_n}\right)\right)}{2 - \exp\left(-\frac{\nu_{el}}{2\nu_n}\right)} \quad (12)$$

The electronic frequency is given by eq 13.

$$\nu_{el} = \frac{2\pi}{\hbar} \frac{H_{DA}^2}{\sqrt{4\pi\lambda k_b T}} \quad (13)$$

The relevant nuclear frequency is often taken as either an intramolecular vibrational ($100 < \nu_n < 3500 \text{ cm}^{-1}$) or a solvent rotational ($10 < \delta_n < 100 \text{ cm}^{-1}$) frequency.⁷³ Critical insight can be gained by considering the limits of eq 12 and revisiting the definition of a reaction as adiabatic or nonadiabatic. For example, when $\nu_{el} \gg \nu_n$, then $\nu_n \kappa = \nu_n$ with $\kappa = 1$ and adiabatic electron transfer results with a pre-exponential factor of ν_n . At the other extreme, when $\nu_n \gg \nu_{el}$, the pre-exponential factor becomes $\nu_n \kappa = \nu_{el}$ and the extent of adiabaticity is limited by the electronic frequency. The Landau–Zener formalism indicates the importance of nuclear and electronic frequencies as critical criteria for the assignment of a reaction as adiabatic ($\kappa = 1$) or nonadiabatic ($\kappa \ll 1$). The practical result of the Landau–Zener approach is that it provides the nonadiabatic criteria of k_{ET} scaling with H_{DA}^2 , while also indicating that an adiabatic reaction becomes independent of H_{DA} . Further, it identifies the rate limits for electron transfer and provides additional physical intuition and an alternative explanation of the Eyring expression for electron transfer, eq 14.

$$k_{ET} = \kappa \frac{k_b T}{h} \exp\left(-\frac{\Delta G^\ddagger}{k_b T}\right) = \kappa \nu_n \exp\left(-\frac{\Delta G^\ddagger}{k_b T}\right) \quad (14)$$

In a nonadiabatic regime, electron transfer is limited by a low probability of hopping from the reactant to the product surface due, in part, to poor orbital overlap. In this situation, nuclear frequencies are much larger than electronic ones, and the reaction does not spend much time in the transition-state region before relaxing back to the reactant minimum, see Figure 5 (sudden electron transfer). An adiabatic reaction is more complicated as the electronic frequency becomes similar to, or surpasses, the magnitude of the nuclear frequency. In this situation, electronic motion becomes dependent on nuclear motion of both the solute and solvent.^{74,75} Moreover, the Born–Oppenheimer approximation is violated for an adiabatic reaction as nuclear and electronic motions become correlated. In practice, the maximal rate constant is often dictated by the nuclear frequency, see Figure 5 (gradual electron transfer).

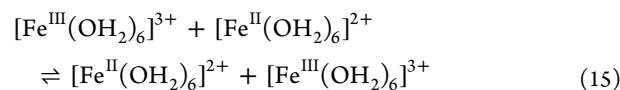
The utility of these theoretical constructs has been demonstrated by critical experimental investigations that date back to the 1950s and remain a fascinating topic presently. In the following sections, some seminal examples and modern advances are discussed in the context of the groundwork laid throughout the beginning part of this article.

PERSPECTIVES ON THE ELECTRON TRANSFER LITERATURE

There now exists a large body of literature that has tested Marcus theory experimentally. In many such experiments, the goal was to fix two of the three Marcus parameters and systematically vary the third. Marcus theory provides a clear description of what should occur when only one or two variables in eq 1 are modified. In general this approach was most successful when the electronic coupling was small and nonadiabatic electron transfer resulted. As the reactions become more adiabatic, it is difficult to disentangle the Marcus parameters, providing some confusion in the literature that warrants further study. In the following sections, examples focusing on individual Marcus parameters are presented. More nuanced examples where λ , H_{DA} , and ΔG^\ddagger are intertwined are also discussed to highlight experimental challenges common in this area of research.

Gibbs Free Energy Change, ΔG^\ddagger

Self-Exchange Electron Transfer. Outer-sphere, self-exchange-type reactions where the products and reactants differed by only one electron have, by definition, $\Delta G^\ddagger = \Delta H^\ddagger = \Delta S^\ddagger = 0$. A classic example reaction is $[\text{Fe}^{\text{III}/\text{II}}(\text{OH}_2)_6]^{3+/2+}$ self-exchange that has been studied extensively, eq 15.^{76–78} A quantitative reaction coordinate has been established providing compelling evidence that electron transfer occurs when the $\text{Fe}^{\text{III}}-\text{O}$ and $\text{Fe}^{\text{II}}-\text{O}$ bond lengths that differ by 0.13 Å are equal in the transition state.^{79,80}



Corresponding reduced force constants, f_j , for the inner-sphere modes of $\text{Fe}-\text{O}$ bonds are about 200 N m^{-1} .⁸¹ Application of eq 5 to the reduced force constants and bond-length changes implies a substantial inner-sphere contribution, $\lambda_i = 1.25 \text{ eV}$, while eq 6 provides $\lambda_o = 1.15 \text{ eV}$. Electronic coupling directly between the iron centers has been estimated computationally,

Table 1. Calculated Self-Exchange and Cross-Reaction Parameters^a

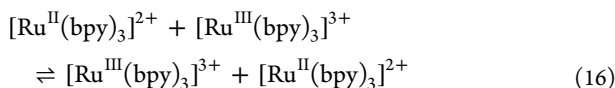
param	$[\text{Fe}^{\text{III}/\text{II}}(\text{OH}_2)_6]^{3+/2+}$	$[\text{Ru}^{\text{III}/\text{II}}(\text{bpy})_3]^{3+/2+}$	$\text{Ru}^{\text{III}} + \text{Fe}^{\text{II}}$ ^a
$r, \text{\AA}$ (+2) [$f, \text{N m}^{-1}$]	3.52 [160]	5.9 [N/A]	
$r_2, \text{\AA}$ (+3) [$f, \text{N m}^{-1}$]	3.39 [250]	5.9 [N/A]	
$\Delta x (\text{\AA})$	0.13	0	0.13
no. of bonds	12	12	6
$\lambda_i (\text{eV})$	1.25	0	0.62
$\lambda_o (\text{eV})$	1.16	0.67	0.97
$\Delta G^\circ (\text{eV})$	0	0	-0.5
$\Delta G^\ddagger (\text{eV})$	0.60	0.17	0.19
$H_{\text{DA}} (\text{cm}^{-1}, \text{eV})$	30, 0.0037	100, 0.012	55, 0.0068
κ_{el}	0.012	0.9	0.05
$k_{\text{ET}}^{\text{calc}} (\text{s}^{-1})$	9	1.1×10^9	4×10^8
$k_{\text{ET}}^{\text{cross}} (\text{s}^{-1})$		-	3×10^8
$k_{\text{ET}}^{\text{expt}} (\text{s}^{-1})$	50	4.9×10^8	2×10^7
$k_{\text{expt}}/k_{\text{calc}}$	5.5	0.4	0.05

^aThe balanced electron transfer reaction is given in eq 17.

$H_{\text{DA}} = 30 \text{ cm}^{-1}$, at a distance where the reaction is most probable.^{82,83}

These collective data provide a clear path for determination of the electron transfer barrier $\Delta G^\ddagger = \lambda/4$, eq 7, and rate constant k_{ET} .⁸⁴ Application of nonadiabatic Marcus theory, eq 2, yields $k_{\text{ET}}^{\text{calc}} = 9 \text{ s}^{-1}$ while experimentally determined rate constants were found to be $k_{\text{ET}}^{\text{expt}} = 50 \text{ s}^{-1}$, and $k_{\text{expt}}/k_{\text{calc}} = 5.5$.⁷⁹ The substantial inner- and outer-sphere contributions and the relatively weak electronic coupling inhibit electron transfer which aids in an assignment of the reaction as *nonadiabatic*.⁸⁵ Note that for simplicity the discussion of the association constant, K_A , for a bimolecular reaction has been excluded. A detailed discussion of the association constant is presented in detail elsewhere.^{86,87}

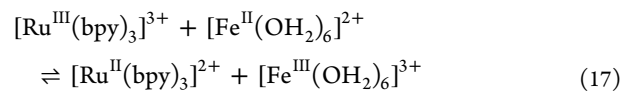
However, not all outer-sphere reactions are nonadiabatic. Inspection of eq 2 indicates that minimizing Δd and maximizing the reactant radii decreases λ which can greatly increase the self-exchange rate constant. A reaction of this type is self-exchange between $[\text{Ru}(\text{bpy})_3]^{2+}$ and $[\text{Ru}(\text{bpy})_3]^{3+}$, eq 16.



Crystal structures revealed only a small bond-length change, $\Delta d = 0.004 \text{ \AA}$, and a negligible inner-sphere reorganization.^{88,89} In addition, the larger radii of $[\text{Ru}(\text{bpy})_3]^{3+/2+}$ relative to $[\text{Fe}(\text{OH}_2)_6]^{3+/2+}$ decreases the magnitude of λ_o . Together, this lowers the total reorganization energy to predominantly an outer-sphere contribution, $\lambda_o = 0.67 \text{ eV}$. Further, $d\pi \rightarrow \pi^*$ back-bonding places significant charge density on the bipyridine ligands which serves to increase H_{DA} .²⁴ Intramolecular electron transfer between aliphatically bridged Ru-metal centers provided estimates of $H_{\text{DA}} \approx 100 \text{ cm}^{-1}$.^{50,90,91} A calculated rate constant based on these parameters is $k_{\text{ET}}^{\text{calc}} = 1.1 \times 10^9 \text{ s}^{-1}$, which compares well with the experimental value $k_{\text{ET}}^{\text{expt}} = 4.9 \times 10^8 \text{ s}^{-1}$, $k_{\text{expt}}/k_{\text{calc}} = 0.4$.⁹² Remarkably, the $[\text{Ru}(\text{bpy})_3]^{3+/2+}$ self-exchange reaction is 8 orders of magnitude larger than that for $[\text{Fe}(\text{OH}_2)_6]^{3+/2+}$, behavior largely due to the smaller barrier that results from a decreased reorganization energy.⁹³ Despite an outer-sphere mechanism, the reaction is assigned as *adiabatic*.²⁴ It is important, however, to emphasize that the magnitude of the rate constant alone is not the only defining feature of an adiabatic reaction as ΔG°

also contributes to the magnitude of ΔG^\ddagger for non-self-exchange electron transfer.⁶⁰

A key question which arises now is of what importance are self-exchange rate constants beyond describing a reaction where the reactants and products are equivalent? One answer to this question lies in the Marcus *cross-relation* that allows electron transfer rate constants to be estimated from self-exchange rate constants. For example, it may be of interest to estimate the rate constant for the reaction of $[\text{Ru}^{\text{III}}(\text{bpy})_3]^{3+}$ with $[\text{Fe}^{\text{II}}(\text{OH}_2)_6]^{2+}$ with knowledge of the two unique self-exchange rate constants, eq 17.⁹⁴



The cross-relation arises, in part, from the expectation that the reorganization energies for a cross-reaction, λ_{12} , are weighted averages of the reorganization energies for self-exchange reactions, λ_{11} and λ_{22} , eq 18, or from thermodynamic considerations.

$$\lambda_{12} = \frac{1}{2}(\lambda_{11} + \lambda_{22}) \quad (18)$$

Correspondingly, rate constants for electron transfer between asymmetric redox couples ($\Delta G^\circ \neq 0$), k_{12} , can be predicted from the corresponding self-exchange rate constants, k_{11} and k_{22} , and the equilibrium constant K_{eq} with f frequently set equal to unity, eq 19.^{81,93,98} A mathematical expression for f exists, eq 20, and accounts for deviations of f from unity, where a collision frequency, $Z \approx 10^{11} \text{ s}^{-1}$, is used.⁹⁹

$$k_{12} = (k_{11}k_{22}K_{\text{eq}}f)^{1/2} \quad (19)$$

$$\ln(f_{12}) = \frac{\ln(K_{\text{eq}})^2}{4\ln\left(\frac{k_{11}k_{22}}{Z^2}\right)} \quad (20)$$

The cross-relation also provides methods to compute electronic coupling between cross-reactions though eq 21. It assumes an average of the force constants for either redox couple and a weighted electronic coupling component.¹⁰⁰

$$H_{\text{DA}}^{12} = \sqrt{H_{\text{DA}}^{11}H_{\text{DA}}^{22}} \quad (21)$$

Either eq 19 or a combination of experimental data with previously described relations can be used to calculate k_{ET} . In either case, application to the reaction $\text{Fe}(\text{H}_2\text{O})_6^{2+} + \text{Ru}(\text{bpy})_3^{3+}$ yields calculated rate constants of $k_{\text{ET}}^{\text{Cross}} = 3 \times 10^8 \text{ s}^{-1}$ while an experimental measurement provided $k_{\text{ET}}^{\text{expt}} = 2 \times 10^7 \text{ s}^{-1}$, and $k_{\text{expt}}/k_{\text{calc}} = 0.05$.^{98,101} This relatively poor agreement likely emanates from the fact that the mechanisms of the two self-exchange reactions are different; $\text{Fe}^{\text{III}/\text{II}}$ exchange occurs nonadiabatically while $\text{Ru}^{\text{III}/\text{II}}$ occurs adiabatically. Indeed, a value of $f \approx 0.03$ for this cross-reaction is ascribed principally to the different transmission coefficients for the two self-exchange reactions, eq 12, which are not included in eq 20. Further, the value of k_{12} calculated with eq 19 is relatively insensitive to the magnitude of Z , changing by a factor of 3 from $Z = 1 \times 10^{10}$ to $1 \times 10^{12} \text{ s}^{-1}$. Parameters for each reaction are tabulated in Table 1.

An extensive database of self-exchange rate constants has been provided by Hupp and Weaver.¹⁰¹ Nevertheless, the ratio of experimental and calculated self-exchange rate constants, $k_{\text{expt}}/k_{\text{calc}}$, typically being less than 10 is manifestly quite remarkable.

Electron Transfer Reactions with Changes in ΔG° .

Rehm and Weller reported fluorescence quenching experimental data in a seminal study of bimolecular electron transfer reactions which did not provide evidence for the Marcus inverted region.^{102,103} Researchers since have concluded that the inverted region was absent for a variety of reasons that include diffusional limitations, excited-state quenching pathways which did not involve electron transfer, and the formation of excited-state products.^{104–106} In now classical experiments, Closs and Miller provided the first experimental demonstration of the Marcus inverted kinetic region.¹⁰⁷ Their approach was to covalently link a donor and acceptor at opposite ends of the saturated steroid bridge shown in Figure 6C. In these D–B–A molecules, the free energy, ΔG° , was varied between 0 and -2.5 eV by using a biphenyl donor and a series of electron acceptors. The magnitude of ΔG° was determined through electrochemical measurements and eq 1. First-order kinetic rate constants measured as a function of $|\Delta G^\circ|$ increased, reached a maximum, and then subsequently decreased. Over the entire free energy range investigated, the rate constants spanned about 3 orders of magnitude.

The critical data is replotted in Figure 6 with an overlaid fit to the nonadiabatic Marcus expression in red, eq 2. The top of the Marcus curve corresponds to the condition $\lambda = -\Delta G^\circ$ that is termed “activationless” electron transfer. Note, however, that the overlaid Marcus fit indicates a steeper parabolic dependence on $-\Delta G^\circ$ in the inverted region than that measured experimentally. This behavior was attributed to a quantum mechanical effect where vibrational energy levels of the acceptor provided sufficient coupling with the donor wave function that electron tunneling occurs through the free energy barrier. A more detailed expression, eq 22, accounts directly for the Franck–Condon weighted density of states by summation over each vibrational mode (w) and incorporates the energy of each vibrational mode, $E = wh\nu$ energy change for the reaction. This quantum mechanical expression adequately modeled the data and revealed the inverted behavior as predicted by Marcus.¹⁰⁸

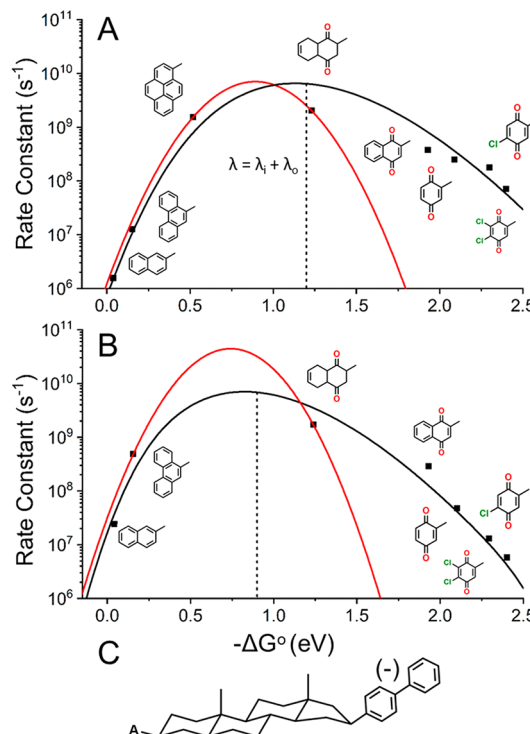


Figure 6. Demonstration of the Marcus inverted region through intramolecular electron transfer. Rate constants, k_{ET} , for electron transfer show a quadratic dependence on the corresponding free energy change, ΔG° , at fixed geometric distance, R_{DA} . Unimolecular electron transfer rate constants determined in 2-methyltetrahydrofuran (A) and di-n-butylether (B). (C) D–B–A molecules studied by Closs and Miller. The acceptor, A, identities are shown with each data point in the plots shown in panels A and B. (A, B) Red parabolas correspond to fits to the experimental data with eq 2 which does not adequately describe reactions deep in the Marcus inverted region; note the deviation when $-\Delta G^\circ > 1.5 \text{ eV}$. Black asymmetric parabolas correspond to a quantum mechanical treatment that includes a modified Franck–Condon factor and vibrational overlap contributions, eq 22. In each case, $\lambda_i = 0.15 \text{ eV}$, which allows for the solvent dependence of λ_o to be quantified, (A) $\lambda_o = 1.1 \text{ eV}$ and (B) $\lambda_o = 0.8 \text{ eV}$. Data reconstructed from ref 107.

$$k_{\text{ET}} = \frac{2\pi}{\hbar} \frac{H_{\text{DA}}^2}{\sqrt{4\pi\lambda k_b T}} \sum_{w=0}^{\infty} \frac{e^{-S^w}}{w!} \exp\left(-\frac{(\Delta G^\circ + \lambda_i + wh\nu)^2}{4\lambda k_b T}\right)$$

$$S = \frac{\lambda_i}{h\nu} \quad (22)$$

Alongside verification of inverted behavior was the observation that the maximum rate constant achieved was solvent-dependent. Dielectric continuum theory predicts that, as solvent dielectric constants decrease, so too does the magnitude of the outer-sphere reorganization energy. In accordance with the numerical results of eq 6, values of λ_o varied over 0.6 eV, ranging from $\lambda = 1.2 \text{ eV}$ (methyltetrahydrofuran) to 0.6 eV (isooctane), thus translating the Marcus parabola maxima with the predicted values of λ , Figure 6. Inner-sphere reorganization energies were small and solvent-independent, $\lambda_i = 0.15 \text{ eV}$, indicating that solvent dielectric properties predominantly controlled the free energy barrier at the maximum rate constant when $\lambda \approx -\Delta G^\circ$.

Ultimately, the seminal work of Closs and Miller ushered in an era where covalently linked donor–bridge–acceptor compounds were used to explore the inverted region. In these studies, a primary goal was to fix λ and vary H_{DA} or $-\Delta G^\circ$. In most cases the inverted kinetic region showed a fall-off with $-\Delta G^\circ$ that was considerably less parabolic than that predicted by Marcus through eq 2. An exception to this was a remarkable demonstration by Gray and co-workers who reported photoinduced electron transfer in bimetallic Ir complexes in CH_3CN solutions.¹⁰⁹ The range of $-\Delta G^\circ$ spanned 1.8 eV, and the rate constants for electron transfer spanned nearly 5 orders of magnitude, between 3.5×10^6 and $1.1 \times 10^{11} \text{ s}^{-1}$ with $\lambda = 1.06 \text{ eV}$ at a fixed distance of 5.8 Å. The apparent agreement with semiclassical Marcus theory in both the normal and inverted regions was stunningly good.

Reorganization Energy, λ

Electron transfer accompanied by large reorganization energies represents an important class of reactions in biology and chemistry. In principle, a conformational change can be rate-limiting, and in such cases, “gated” electron transfer may result.^{110–113} Some time ago, Vallee and Williams described the possibility of an “entactic state” where a metal ion present in an intermediate geometry lowered the inner-sphere reorganization energy and hence facilitated electron transfer.^{114,115} In practice, it has proven to be most difficult to control λ independently without also influencing the other two Marcus parameters.¹¹⁶

Electronic Coupling Matrix Element, H_{DA}

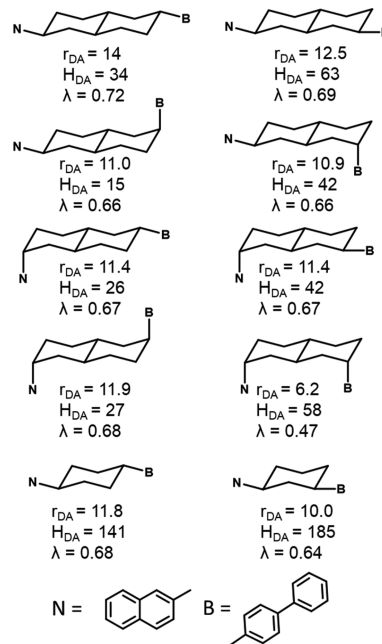
Distance-Dependent Electron Transfer, H_{DA} Entangled with λ . Electron transfer rate constants for D–B–A compounds where the length of a rigid bridge is varied have historically been a means to extract the D–A electronic coupling magnitude, H_{DA} . A complicating aspect of this approach is that the outer-sphere reorganization energy is also distance-dependent as is evident from eq 6. Further, λ is expected to decrease as redox centers become more coupled, a consequence of delocalization altering the equilibrium bond length and electron density distributions.⁴⁷ Nevertheless, disentangling the contributions from H_{DA} and λ on the measured kinetics is nontrivial and generally has been accomplished using theoretical expectations based on dielectric continuum theory.

Interestingly, the number of steroidal bridge units and the stereochemical substitution of the donor and acceptor in the classical Closs–Miller experiments provided variable distance at a fixed driving force ($\Delta G^\circ \approx -0.05 \text{ eV}$), Scheme 2. An approximately 2 orders of magnitude change in rate constant was reported that is impressively similar to those achieved by varying the driving force alone.¹¹⁷

Such results verifiably demonstrate the dramatic effect that distance and donor–acceptor geometry have on electron transfer.^{113,118} After correcting for the distance dependence of λ , H_{DA} was determined for each compound. Plotting $\ln(H_{\text{DA}})^2$ vs R_{DA} for compounds with similar equatorial/equatorial stereochemistry provided $\beta = 1.1 \text{ \AA}^{-1}$, which has been shown to be quite general for reactions occurring through aliphatic C–C bonds.

However, the magnitude of β in many biological electron transfer reactions is sensitive to protein secondary and tertiary structures, $\beta = 1.1 \text{ \AA}^{-1}$, while experimental work on DNA hairpins has shown $\beta = 0.64 \text{ \AA}^{-1}$.^{119–124} Others have demonstrated relatively weak distance dependencies for

Scheme 2. Stereochemical and Substitutional Control of Donor–Acceptor Distance, Electronic Coupling, and Reorganization Energy in Compounds Containing an Aliphatic Steroidal Spacer^a



^aMolecules adapted with permission from ref 117. Copyright 1986 American Chemical Society. Units of R_{DA} Å; H_{DA} , cm⁻¹; λ , eV.

electron transfer over long distances in porphyrins, $\beta = 0.4 \text{ \AA}^{-1}$.^{118,125,126} Some reports and models suggest extremely steep distance dependencies for electron transfer through vacuum, $\beta > 2.5 \text{ \AA}^{-1}$, or nonpolar solvents, $1.2 < \beta < 1.7 \text{ \AA}^{-1}$. Distance dependencies of electron transfer occurring through alkane bonds, $\beta \sim 1.0 \text{ \AA}^{-1}$, are larger than experimental studies of phenylenevinylene bridges by Wasielewski and co-workers which demonstrated remarkably weak distance dependencies, $\beta = 0.04 \text{ \AA}^{-1}$.^{127–129}

The distance dependence of the reorganization energy in the inverted region was quantified by Mallouk and co-workers for a series of alkane-bridged Ru(bpy)₃–viologen complexes, Figure 7A. Rate constants spanned a factor of 30 (from $5 \times 10^9 \text{ s}^{-1}$ to $2 \times 10^{11} \text{ s}^{-1}$) over a driving force range of $-0.5 < \Delta G^\circ < -1.5 \text{ eV}$.¹³⁰ Excited-state electron transfer to the viologen fell in the Marcus normal region while back electron transfer ($\text{MV}^{+} \rightarrow \text{Ru}^{\text{III}}$) fell in the inverted region with reorganization energies of 0.7 and 1 eV, respectively, Figure 7B. Increasing the number of CH_2 groups from 1 to 2 did not result in a pronounced distance dependence in the Marcus normal region as H_{DA} was found to be constant, $H_{\text{DA}} = 23 \text{ cm}^{-1}$. However, rate constants in the inverted region were found to be weakly distance-dependent, with H_{DA} decreasing from 34 cm^{-1} for $n = 1$ and 2 , respectively.¹³¹

Additional studies varied the Ru(bpy)₃²⁺–viologen separation by over 9–17 Å with saturated $(\text{CH}_2)_n$ ($n = 1–5, 7, 8$) spacers.¹³² The distance dependence for $n < 5$ (9–13 Å) followed the predicted exponential dependence of eq 8 while for $n = 7$ or 8 a markedly different dependence was observed, implying a change in mechanism from *through-bond* to *through-space* due to the conformational flexibility of $(\text{CH}_2)_{7,8}$. When these compounds were complexed with cyclodextrin the *through-space* pathways were effectively removed and

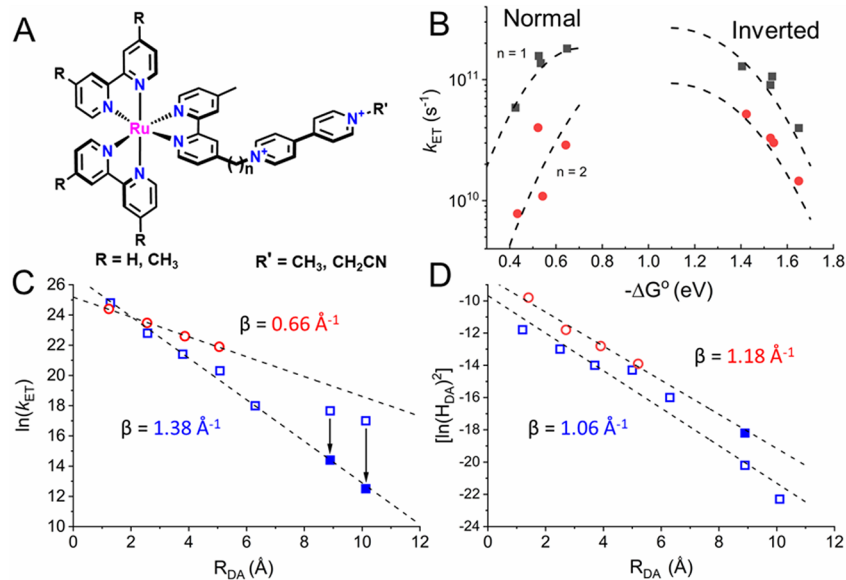


Figure 7. (A) $\text{Ru}(\text{bpy})^{2+}-\text{(CH}_2)_n-\text{methyl viologen D-B-A}$ molecules studied by Mallouk and co-workers in CH_3CN . (B) Marcus parabolas for normal ($-\Delta G^\circ < 1 \text{ eV}$) and inverted ($-\Delta G^\circ > 1 \text{ eV}$) electron transfer for $(\text{CH}_2)_n$ black ($n = 1$) and red ($n = 2$). (C) Effect of distance on the electron transfer rate constant without correcting for $\lambda(R_{\text{DA}})$. Attenuation factors $\beta = 1.38 \text{ \AA}^{-1}$ and $\beta = 0.66 \text{ \AA}^{-1}$ correspond to the forward (normal) and back (inverted) reaction, respectively. Solid squares correspond to cyclodextrin encapsulated compounds to remove through-space electron transfer pathways. (D) Calculated values of H_{DA} as a function of R_{DA} after application of eq 8 and 9 to determine λ for each D-B_n-A couple. Resulting quantities reflect attenuation factors, β , that are equal for the normal and inverted reactions. Data reproduced from refs 130 and 132.

exponential behavior consistent with $n = 1-5$ was observed. Electron transfer in the inverted region was found to be less sensitive to distance, $\beta = 0.66 \text{ \AA}^{-1}$, than in the normal region, $\beta = 1.38 \text{ \AA}^{-1}$. However, the initial analysis assumed a constant reorganization, and when this was accounted for, it was found that λ increased by as much as 0.35 eV as R_{DA} increased from 9 to 16.8 Å. Employing eq 6 to determine λ for each complex provided $\beta = 1.1 \pm 0.1 \text{ \AA}^{-1}$, concluding that the distance dependences were similar for electron transfer in both kinetic regions.

Distance-Dependent Electron Transfer Entangled with λ and ΔG° . A sophisticated distance-dependence may exist for λ and H_{DA} . An initial expectation is that with increasing D-A distance the increase in λ occurs alongside a simultaneous decrease in H_{DA} . This highlights the fact that a Marcus parabola is ultimately a function of both variables, Figure 8.

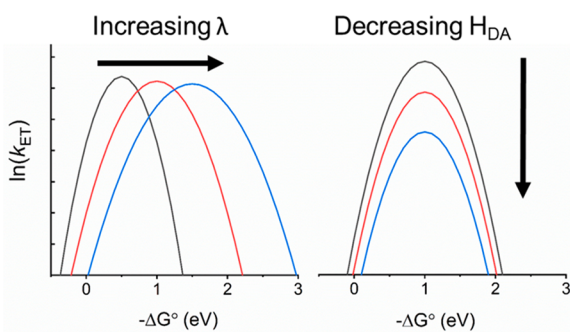


Figure 8. Effects of increasing reorganization energies and decreasing electronic coupling on Marcus parabolas for electron transfer. An increase in the reorganization energies forces the parabola to translate to the right, maintaining the maxima at $\Delta G^\circ = \lambda$. Decreases in electronic coupling cause the maximum rate constant to decrease at a fixed λ value.

Because of the unique distance dependencies of λ and H_{DA} as predicted by eqs 6 and 8, a systematic distance-dependent study of intramolecular electron transfer kinetics within a series of complexes with similar driving forces and bridge structure would enable one to deconvolute the effects of each Marcus parameter on k_{ET} . Such a study was carried out by Wenger and co-workers, who characterized a series of donor-acceptor compounds bearing a substituted triphenylamine (TPA) donor and an anthraquinone (AQ) acceptor linked by 1, 2, or 3 *p*-xylene spacers to a $\text{Ru}(\text{bpy})_3$ core, Figure 9.^{116,133} The distance between the TPA and AQ was 22 Å ($n = 1$), 26 Å ($n = 2$), and 39 Å ($n = 3$). Further, ΔG° was controlled with functional groups that tuned the $E^\circ(\text{TPA}^{+/\circ})$ formal reduction potential. Photoexcitation of $\text{Ru}(\text{bpy})_3$ resulted in electron transfer and the formation of $\text{TPA}^+-\text{B}-\text{AQ}^-$. Comprehensive kinetic analyses were carried out with complexes that had fixed R_{DA} distances and tuned ΔG° values and for those with fixed ΔG° and a different number of xylene spaces. Marcus parameters garnered from the temperature-dependent transient spectroscopic studies are provided in Table 2.

This data highlights an unexpected result. A maximum rate constant was observed at an intermediate electron transfer distance; i.e., electron transfer occurred more rapidly in compound II than it did in I or III. For compound IIB, $k_{\text{ET}} = 7.4 \times 10^6 \text{ s}^{-1}$, while for either IB or IIIB, $k_{\text{ET}} = 2.3 \times 10^6 \text{ s}^{-1}$ on average. Such an observation was puzzling yet was supported by internal comparisons at constant R_{DA} . For example, when $R_{\text{DA}} = 22 \text{ \AA}$, k_{ET} varied only slightly across the substituted TPA series, from 3 to $7 \times 10^5 \text{ s}^{-1}$. Similar effects were found when $R_{\text{DA}} = 31$ or 39 Å.

Temperature-dependent kinetic data provided ΔG^\ddagger from which λ was determined, eq 7. In each case, the expected distance dependence for λ was observed and λ increased from ~1 eV at 22 Å to ~2 eV at 34 Å (Table 1). Comparison of λ and ΔG° revealed that, at a fixed distance, electron transfer

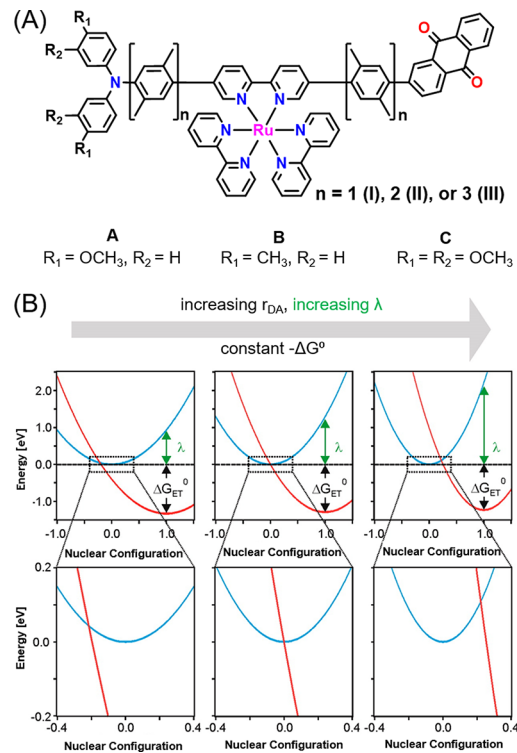


Figure 9. (A) TPA–Ru(bpy)₃–AQ triad molecules studied by Wenger and co-workers. Substituents on the distal phenyl rings of the TPA unit allow for independent tuning of ΔG° , and distinguish the molecules into three classifications, A, B, and C. Each class of donor–acceptor molecules are distance controlled by the substitution of $n = 1$, 2, or 3 *p*-xylene groups across the Ru(bpy)₃ photosensitizer. (B) Schematic Marcus parabola diagrams for short (26 Å), intermediate (31 Å), and long distance (39 Å) electron transfer. Parabolas show the possibility that the interplay of λ , H_{DA} , and r_{DA} provides unique Marcus surfaces for each mechanism (inverted, activationless, and normal) which permit the observation of rate maxima at intermediate distances. Adapted with permission from ref 116. Copyright 2016 American Chemical Society.

occurred either in the inverted, activationless, and normal regimes, Figure 9B.¹³⁴ Furthermore, H_{DA} values extracted from the kinetic data were small and relatively insensitive to distance, a finding contrary to previous studies of *p*-xylene wires where $\beta \approx 0.7$.^{135,136} The magnitudes of H_{DA} indicated that the reaction was distinctly nonadiabatic. At a fixed ΔG° , activationless electron transfer occurred at intermediate distances, indicated by larger rate constants while Marcus normal kinetics were observed at extreme distances.¹³⁷ Hence, this work highlights a fascinating interplay between λ and k_{ET} that has continued to provide additional insight into electron transfer reactivity.¹³⁸

Table 2. Free Energies, Reorganization Energies, and Electronic Coupling values for TPA–Ru(bpy)₃–AQ Triads

n (Å)	A			B			C			ET type ^c
	ΔG° ^a	λ ^a	H_{DA} ^b	ΔG° ^a	λ ^a	H_{DA} ^b	ΔG° ^a	λ ^a	H_{DA} ^b	
I (22)	−1.3	0.9	0.11	−1.5	1.2	0.12	−1.3	0.9	0.10	I
II (31)	−1.3	1.3	0.14	−1.5	1.5	0.18	−1.3	1.3	0.10	A
III (39)	−1.2	2.2	0.10	−1.4	2.0	0.10	−1.2	2.3	0.11	N

^aUnits of eV. ^bUnits of cm^{−1}. Values contain uncertainties of ± 0.03 . ^cType of electron transfer reaction, I = inverted, A = activationless, N = normal. See Figure 2.

Mixed-Valence Complexes and Intervalence Charge Transfer. As described previously, strong electronic coupling in class II or III mixed-valent compounds can lead to intervalence charge transfer (IVCT) absorption bands observed at $E_{\text{op}} = \lambda + \Delta G^\circ$ with extinction coefficients >50 M^{−1}cm^{−1}.⁹¹ The late Noel Hush derived a relationship between band intensities, positions, and widths, eq 11, that relies on knowledge of the electron transfer distance. Indeed, IVCT band analysis provides most of the experimental values of H_{DA} found in the literature. These steady-state spectroscopic properties are convenient for experimental determination of H_{DA} with the Mulliken–Hush equation.

While there were early reports of such transitions in mixed-valent bisferrocene compounds and in pigments, such as Prussian blue, a classical example of mixed-valence chemistry is $[(\text{NH}_3)_5\text{Ru}^{\text{II}}(\text{pz})\text{Ru}^{\text{II}}(\text{NH}_3)_5]^{4+}$, the Creutz–Taube ion, where pz is pyrazine, Figure 10.¹⁴⁰

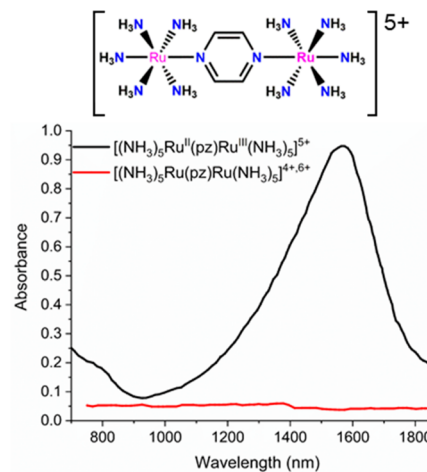


Figure 10. (Top) Structure of the Creutz–Taube ion, $(\text{NH}_3)_5\text{Ru}^{\text{II}}(\text{pz})\text{Ru}^{\text{III}}(\text{NH}_3)_5$. (Bottom) Near infrared spectra of the ground (+4) state and doubly oxidized (+6) state (red line), and the mixed-valent ($\text{Ru}^{\text{II}}-\text{Ru}^{\text{III}}, +5$) state (black line). Intense absorption at 1570 nm is assigned as the IT transition between Ru^{II} and Ru^{III} . Data reproduced from ref 140.

An intense absorption feature unique to the mixed-valent $\text{Ru}^{\text{II}}-\text{Ru}^{\text{III}}$ state at 1570 nm was assigned as the IVCT $\text{Ru}^{\text{II}}-\text{B}-\text{Ru}^{\text{III}} \rightarrow \text{Ru}^{\text{III}}-\text{B}-\text{Ru}^{\text{II}}$. This early demonstration resulted in the subsequent report of literally thousands of symmetric and asymmetric mixed-valent complexes, the data from which Robin and Day later used to establish the classifications provided in Figure 4. As fate would have it, the Robin–Day assignment of the Creutz–Taube ion as a delocalized (class III) or a valence-localized (class II) compound still remains somewhat uncertain.^{43,141–144}

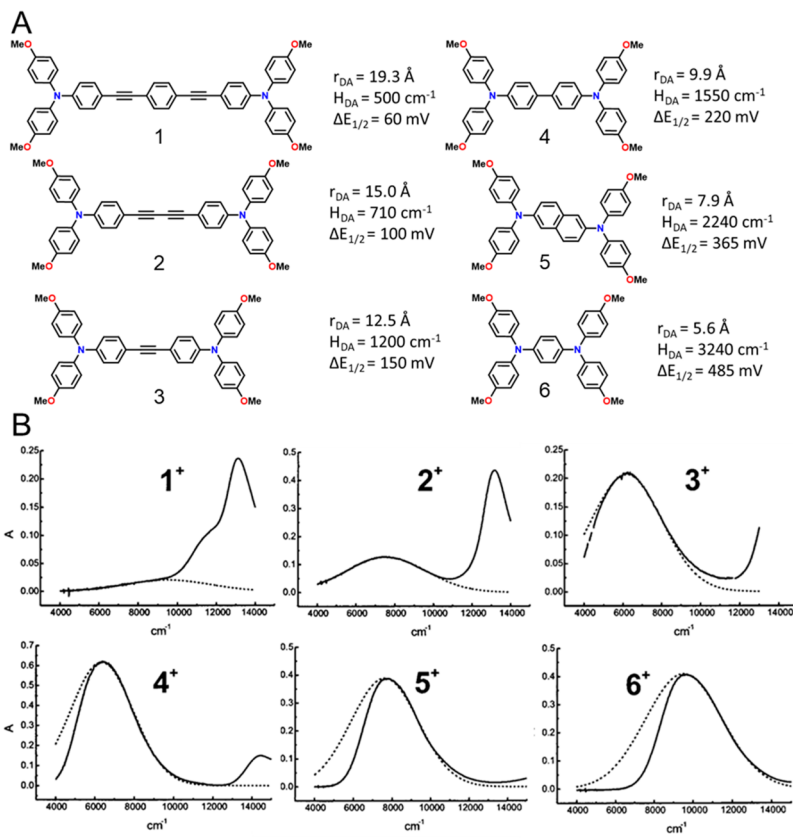


Figure 11. (A) Bis-triarylaminies studied by Lambert and Nöll. Text to the right of the molecules describes the geometric charge transfer distance, electronic coupling, and electrochemical splitting. (B) UV–vis–NIR spectra of the one-electron oxidized compounds (—). Overlaid on the data are simulated Gaussian-shaped bands (...) used, in part, to calculate H_{DA} . Note that the data and simulated Gaussian bands are similar in shape for the low-energy bands in compounds 1^+ , 2^+ , and 3^+ , while for compounds 4^+ , 5^+ , and 6^+ the low-energy IVCT bands are significantly attenuated as $E_{\text{op}} < 2H_{\text{DA}}$. For these complexes, H_{DA} is given by $E_{\text{op}}/2 = \lambda/2$. Molecules were reproduced from ref 51. Data were adapted from ref 51 with permission.

Coupling-Dependent Electron Transfer, ΔG° Entangled with H_{DA} . Experimental evidence for the influence of H_{DA} on electrochemical properties was elegantly demonstrated by Lambert and Nöll in a series of mixed-valent organic compounds with triphenylamine units, Figure 11A.⁵¹ The geometric charge transfer distances spanned from 5.6 to 19.3 Å. Low-energy IVCT transitions were quantified for the one-electron oxidized compounds with an absorption maximum between $6000 \text{ cm}^{-1} < E_{\text{OP}} < 10000 \text{ cm}^{-1}$ and extinction coefficients that increased by a factor of 5 from $4570 \text{ M}^{-1} \text{ cm}^{-1} < \epsilon_{\text{max}} < 22680 \text{ M}^{-1} \text{ cm}^{-1}$.

An interesting result was the identification of asymmetric charge transfer bands for compounds with $R_{\text{DA}} < 10 \text{ \AA}$. An IVCT band shape analysis indicated a shift from class II (compounds **1** and **2**), to borderline class II/III (compounds **3–5**), to class III (compound **6**) behavior made possible by synthetic modification of the bridge, Figure 11B.⁵² This data provides a clear demonstration that the theoretical expectation in class III compounds that optical absorption does not occur when $E_{\text{photon}} < 2H_{\text{DA}}$ is valid. The data also indicated that the electron transfer barrier, ΔG^\ddagger , was sensitive to the coupling for class II/III electron transfer.

A subtle, yet critical, result was that as R_{DA} decreased the electrochemical separation (splitting) between the anodic and cathodic peaks in cyclic voltammograms increased from 60 to 485 mV, Figure 11. The origin of the increased splitting was ascribed to stabilization of the mixed-valent state relative to the

ground-state and two-electron oxidized form of the molecule via the comproportionation constant, eqs 10a and 10b. An alternative explanation considered was that the inductive influence of the first oxidation made the second oxidation more difficult, causing K_c to increase. Many experimental studies of this phenomena have revealed that this is not always the case.^{48,145,146} Indeed, many published works have related reduction potentials to the electronic coupling and to ΔG° ,¹⁴⁷ which is now understood to result in significant errors.¹⁴⁵ As detailed recently by Winter,⁴⁸ the electrochemistry of class II and III molecular complexes is influenced by all three Marcus parameters in a manner that is often difficult if not impossible to disentangle.

To this extent, Kubiak and co-workers have utilized novel IR line broadening techniques¹⁴⁸ which monitor the $\nu(\text{CO})$ stretching frequency as an indicator of electron transfer dynamics in mixed-valent complexes of pyrazine-bridged Ru₃ clusters, Figure 12.^{149–151}

For example, k_{ET} in the mixed-valent state of the symmetric ($\Delta G^\circ = 0$) pyrazine-bridged complex shown ranged from 1×10^9 to $1 \times 10^{11} \text{ s}^{-1}$ when *para* substituents on the pyridine rings were tuned from dimethylamino to cyano.¹⁵¹ Interestingly, despite these inductive substituents being introduced seven atoms away from a common pyrazine bridge, H_{DA} was reported to decrease from 2180 to 1310 cm⁻¹ though IVCT analysis.¹⁵² This degree of coupling is consistent with a nearly delocalized charge, class III, when R = N(CH₃)₂ or H, or a

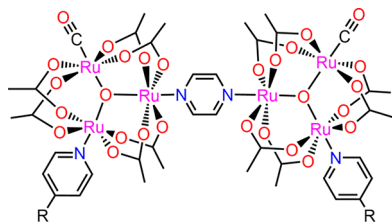


Figure 12. Molecular structure of the pyrazine-bridged Ru_3 clusters studied by Kubiak and co-workers. Adapted with permission from ref 150. Copyright 2013 American Chemical Society.

charge-localized class II complex, for $R = \text{CN}$. Remote ligand control of electronic coupling is not uncommon yet could not have been determined through formal reduction potentials.^{153,154}

Recent studies by Meyer and co-workers investigated electron transfer in cyclometalated Ru^{II} compounds covalently linked through an aryl-thiophene bridge to an organic triphenylamine (TPA) unit, **Figure 13A**. Steric modification

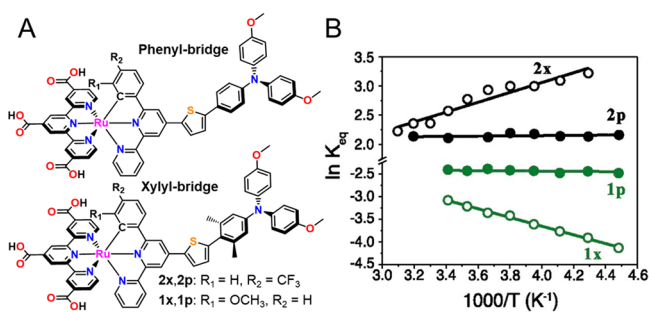


Figure 13. (A) Compounds studied by Meyer and co-workers. Light excitation was used to initiate a $\text{Ru}^{\text{III}}-\text{B}-\text{TPA} \rightarrow \text{Ru}^{\text{II}}-\text{B}-\text{TPA}^+$ equilibrium. Forward, k_1 , and reverse, k_{-1} , rate constants were quantified to determine K_{eq} . (B) van't Hoff analysis of the equilibrium data reveals a marked temperature dependence of K_{eq} for $1x$ and $2x$, consistent with nonadiabatic electron transfer. Temperature-independent values of K_{eq} ($1p$ and $2p$) correspond to an adiabatic electron transfer equilibrium. Structures adapted with permission from ref 155. Copyright 2018 American Chemical Society. Data for part B from ref 156.

allowed electronic coupling to be tuned drastically without a significant change in the D–A geometric distance: when $B = \text{phenyl}$, H_{DA} was found to be 1000 cm^{-1} ; when $B = \text{xyllyl}$, $H_{\text{DA}} < 150 \text{ cm}^{-1}$, as evidenced by the appearance of an intense and a weak IVCT transition, respectively.¹⁵⁵ The methyl groups on the xyllyl ring prevented planarization of the bridge which disrupted orbital conjugation.

The kinetics for intramolecular, $\text{Ru}^{\text{III}/\text{II}}-\text{B}-\text{TPA}^{+/0}$, electron transfer between the Ru-metal center and TPA unit were quantified as a function of temperature after excited-state injection into TiO_2 . The kinetic data provided K_{eq} values over a 100 degree temperature range. A Van't Hoff analysis revealed a clear distinction between adiabatic and nonadiabatic electron transfer. When H_{DA} was large, temperature-independent K_{eq} values indicated that $\Delta H^\circ = 0$, consistent with no heat transfer at constant pressure, $q_p = 0$, and an *adiabatic* redox equilibrium.^{156,157} In contrast when coupling was weak through the xyllyl bridge, there was a marked enthalpy change consistent with nonadiabatic electron transfer, **Figure 12B**. Therefore, for two inner-sphere redox equilibria a relatively

small 30° change in the aryl-thiophene bridge angle was sufficient to change the mechanism from adiabatic to nonadiabatic. The data provides a clear example of how a subtle structural change can dramatically alter the adiabaticity of electron transfer. Moreover, the magnitude of $|\Delta G^\circ|$ decreased when the electronic coupling was large, showing that H_{DA} and ΔG° can become entangled. These studies point toward the utility of future research of D–B–A compounds where ΔG° is fixed and H_{DA} is systematically controlled through the bridge.

CONCLUSION

Electron transfer theory and experiment remains relevant to many aspects of chemical education and research. Indeed, while the utility of electron transfer has been supported by decades of research dating back to the Closs and Miller experiments, modern educational approaches require the establishment of accessible methods for students and researchers to become acquainted with the field. Herein, a pedagogical introduction to the underlying principles, beginning with the construction of Gibbs free energy surfaces to visualize electron transfer was presented. Three Marcus parameters (λ , H_{DA} , and ΔG°) that define the free energy surfaces were discussed, and a distinction between adiabatic and nonadiabatic electron transfer mechanisms were made that highlighted the impact of strong electronic coupling on the free energy surfaces and electron transfer mechanisms. Practical examples utilizing each of the Marcus parameters were discussed and theory was applied to reliably calculate and estimate electron transfer rate constants which served to demonstrate the validity of Marcus' simple, yet elegant, approach.

AUTHOR INFORMATION

Corresponding Author

*E-mail: gjmeyer@email.unc.edu.

ORCID

Eric J. Piechota: 0000-0003-0835-5423

Gerald J. Meyer: 0000-0002-4227-6393

Notes

The authors declare no competing financial interest.

ACKNOWLEDGMENTS

The authors thanks Renato N. Sampaio and Ludovic Troian-Gautier for fruitful and animated discussions regarding electron transfer. Support for this work was provided through a grant from the Division of Chemical Sciences, Office of Basic Energy Sciences, Office of Energy Research, U.S. Department of Energy (Grant DESC0013461).

REFERENCES

- Pardo, J. Q. Teaching a model for writing Lewis structures. *J. Chem. Educ.* **1989**, *66* (6), 456.
- Nassiff, P.; Czerwinski, W. A. Teaching Beginning Chemistry Students Simple Lewis Dot Structures. *J. Chem. Educ.* **2015**, *92* (8), 1409–1411.
- Kolb, D. The chemical equation. Part II: Oxidation-reduction reactions. *J. Chem. Educ.* **1978**, *55* (5), 326.
- Hall, W. T. Oxidation-reduction reactions. *J. Chem. Educ.* **1929**, *6* (3), 479.

- (5) Matta, C. F.; Gillespie, R. J. Understanding and Interpreting Molecular Electron Density Distributions. *J. Chem. Educ.* **2002**, *79* (9), 1141.
- (6) Smith, P. R.; Richardson, J. W. Electron Density Shifts during Chemical Bond Formation I. *J. Phys. Chem.* **1965**, *69* (10), 3346–3357.
- (7) Taube, H.; Myers, H.; Rich, R. L. Observations on the Mechanism of Electron Transfer in Solution. *J. Am. Chem. Soc.* **1953**, *75* (16), 4118–4119.
- (8) Herzberg, G. *Molecular Spectra and Molecular Structure*, 2nd ed.; D. Van Nostrand Company, Inc.: Princeton, NJ, 1950; Vol. 1, p 658.
- (9) Adamson, A. W. Properties of excited states. *J. Chem. Educ.* **1983**, *60* (10), 797.
- (10) Sutin, N.; Creutz, C. Electron-transfer reactions of excited states. *J. Chem. Educ.* **1983**, *60* (10), 809.
- (11) Isied, S. S. Long-Range Intramolecular Electron Transfer Reactions across Simple Organic Bridges, Peptides, and Proteins. In *Electron Transfer Reactions*; American Chemical Society: Washington, DC, 1997; Vol. 253, pp 331–347.
- (12) Schmehl, R. H.; Schanze, K. S. Applications of Inorganic Photochemistry in the Chemical and Biological Sciences - Contemporary Developments. *J. Chem. Educ.* **1997**, *74* (6), 633.
- (13) Netzel, T. L. Electron Transfer Reactions in DNA. *J. Chem. Educ.* **1997**, *74* (6), 646.
- (14) Marcus, R. A.; Sutin, N. Electron transfers in chemistry and biology. *Biochim. Biophys. Acta, Rev. Bioenerg.* **1985**, *811* (3), 265–322.
- (15) Scott, R. A.; Mauk, A. G.; Gray, H. B. Experimental approaches to studying biological electron transfer. *J. Chem. Educ.* **1985**, *62* (11), 932.
- (16) Meek, S. J.; Pitman, C. L.; Miller, A. J. M. Deducing Reaction Mechanism: A Guide for Students, Researchers, and Instructors. *J. Chem. Educ.* **2016**, *93* (2), 275–286.
- (17) Bolton, J. R.; Archer, M. D., Basic Electron-Transfer Theory. In *Electron Transfer in Inorganic, Organic, and Biological Systems*; American Chemical Society: 1991; Vol. 228, pp 7–23.
- (18) Zusman, L. D. Outer-sphere electron transfer in polar solvents. *Chem. Phys.* **1980**, *49* (2), 295–304.
- (19) Beratan, D. N.; Onuchic, J. N. Adiabaticity and nonadiabaticity in bimolecular outer-sphere charge transfer reactions. *J. Chem. Phys.* **1988**, *89* (10), 6195–6203.
- (20) Bergquist, W.; Heikkinen, H. Student ideas regarding chemical equilibrium: What written test answers do not reveal. *J. Chem. Educ.* **1990**, *67* (12), 1000.
- (21) Van Driel, J. H.; Verloop, N.; de Vos, W. Introducing Dynamic Equilibrium as an Explanatory Model. *J. Chem. Educ.* **1999**, *76* (4), 559.
- (22) Balzani, V.; Bolletta, F.; Gandolfi, M. T.; Maestri, M. In *Bimolecular electron transfer reactions of the excited states of transition metal complexes*; Berlin, Heidelberg, Springer Berlin Heidelberg: Berlin, Heidelberg, 1978; pp 1–64.
- (23) Turro, N. J. R. V.; Scaiano, J. C. *Principles of Modern Photochemistry: An Introduction*; University Science Books: Sausalito, CA, 2009.
- (24) Sutin, N. Nuclear, electronic, and frequency factors in electron transfer reactions. *Acc. Chem. Res.* **1982**, *15* (9), 275–282.
- (25) Marcus, R. A. Tutorial on rate constants and reorganization energies. *J. Electroanal. Chem.* **2000**, *483* (1), 2–6.
- (26) Libby, W. F. Theory of Electron Exchange Reactions in Aqueous Solution. *J. Phys. Chem.* **1952**, *56* (7), 863–868.
- (27) Marcus, R. A. On the Theory of Oxidation-Reduction Reactions Involving Electron Transfer. I. *J. Chem. Phys.* **1956**, *24* (5), 966–978.
- (28) Gerischer, H. Messungen der Austauschstromdichte beim Gleichgewichtspotential an einer PlatinElektrode in $\text{Fe}^{2+}/\text{Fe}^{3+}$ -Lösungen. *Z. Elektrochem. Angew. P.* **1950**, *54* (5), 366–369.
- (29) Gerischer, H.; Willig, F. In *Reaction of Excited Dye Molecules at Electrodes*; Springer: Berlin, 1976; pp 31–84.
- (30) Gerischer, H. Die Austauschstromdichte beim Gleichgewichtspotential an Elektroden mit einem potentialbestimmenden Vorgang. *Z. Elektrochem. Angew. P.* **1950**, *54* (5), 362–365.
- (31) Barbara, P. F.; Meyer, T. J.; Ratner, M. A. Contemporary Issues in Electron Transfer Research. *J. Phys. Chem.* **1996**, *100* (31), 13148–13168.
- (32) Lewis, F. D.; Wu, T.; Liu, X.; Letsinger, R. L.; Greenfield, S. R.; Miller, S. E.; Wasielewski, M. R. Dynamics of Photoinduced Charge Separation and Charge Recombination in Synthetic DNA Hairpins with Stilbenedicarboxamide Linkers. *J. Am. Chem. Soc.* **2000**, *122* (12), 2889–2902.
- (33) Moss, S. J.; Coady, C. J. Potential-energy surfaces and transition-state theory. *J. Chem. Educ.* **1983**, *60* (6), 455.
- (34) Marcus, R. A. Local Approximation of Potential-Energy Surfaces by Surfaces Permitting Separation of Variables. *J. Chem. Phys.* **1964**, *41* (3), 610–616.
- (35) Brunschwig, B. S.; Sutin, N. Energy surfaces, reorganization energies, and coupling elements in electron transfer. *Coord. Chem. Rev.* **1999**, *187* (1), 233–254.
- (36) Skourtis, S. S.; Beratan, D. N.; Onuchic, J. N. The two-state reduction for electron and hole transfer in bridge-mediated electron-transfer reactions. *Chem. Phys.* **1993**, *176* (2), 501–520.
- (37) Zwickl, J.; Shenvi, N.; Schmidt, J. R.; Tully, J. C. Transition State Barriers in Multidimensional Marcus Theory. *J. Phys. Chem. A* **2008**, *112* (42), 10570–10579.
- (38) Marcus, R. A. Electron transfer reactions in chemistry. Theory and experiment. *Rev. Mod. Phys.* **1993**, *65* (3), 599–610.
- (39) Lewis, N. A. Potential energy diagrams: A conceptual tool in the study of electron transfer reactions. *J. Chem. Educ.* **1980**, *57* (7), 478.
- (40) Di Giacomo, F. A Short Account of RRKM Theory of Unimolecular Reactions and of Marcus Theory of Electron Transfer in a Historical Perspective. *J. Chem. Educ.* **2015**, *92* (3), 476–481.
- (41) Fawcett, W. R.; Fawcett, W. R. *Liquids, Solutions, and Interfaces: From Classical Macroscopic Descriptions to Modern Microscopic Details*; Oxford University Press: Cary, NC, 2004.
- (42) Silverstein, T. P. Marcus Theory: Thermodynamics CAN Control the Kinetics of Electron Transfer Reactions. *J. Chem. Educ.* **2012**, *89* (9), 1159–1167.
- (43) Demadis, K. D.; Hartshorn, C. M.; Meyer, T. J. The Localized-to-Delocalized Transition in Mixed-Valence Chemistry. *Chem. Rev.* **2001**, *101* (9), 2655–2686.
- (44) Paddon-Row, M. N. Investigating long-range electron-transfer processes with rigid, covalently linked donor-(norbornylidene bridge)-acceptor systems. *Acc. Chem. Res.* **1994**, *27* (1), 18–25.
- (45) Hush, N. S. Distance Dependence of Electron Transfer Rates. *Coord. Chem. Rev.* **1985**, *64*, 135–157.
- (46) Robin, M. B.; Day, P. Mixed Valence Chemistry—A Survey and Classification. In *Advances in Inorganic Chemistry and Radiochemistry*; Emeléus, H. J., Sharpe, A. G., Eds.; Academic Press, 1968; Vol. 10, pp 247–422.
- (47) Brunschwig, B. S.; Creutz, C.; Sutin, N. Optical transitions of symmetrical mixed-valence systems in the Class II-III transition regime. *Chem. Soc. Rev.* **2002**, *31* (3), 168–184.
- (48) Winter, R. F. Half-Wave Potential Splittings $\Delta E_{1/2}$ as a Measure of Electronic Coupling in Mixed-Valent Systems: Triumphs and Defeats. *Organometallics* **2014**, *33* (18), 4517–4536.
- (49) Sutton, J. E.; Sutton, P. M.; Taube, H. Determination of the comproportionation constant for a weakly coupled mixed-valence system by titration of the intervalence transfer band: .mu.- $(4,4'$ -bipyridyl)-bis(pentaammineruthenium)(S+). *Inorg. Chem.* **1979**, *18* (4), 1017–1021.
- (50) Patoux, C.; Launay, J.-P.; Beley, M.; Chodorowski-Kimmes, S.; Collin, J.-P.; James, S.; Sauvage, J.-P. Long-Range Electronic Coupling in Bis(cyclometalated) Ruthenium Complexes. *J. Am. Chem. Soc.* **1998**, *120* (15), 3717–3725.
- (51) Lambert, C.; Nöll, G. The Class II/III Transition in Triarylamine Redox Systems. *J. Am. Chem. Soc.* **1999**, *121* (37), 8434–8442.

- (52) Lambert, C.; Nöll, G.; Schelter, J. Bridge-mediated hopping or supereexchange electron-transfer processes in bis(triarylamine) systems. *Nat. Mater.* **2002**, *1* (1), 69–73.
- (53) Nelsen, S. F. Almost Delocalized” Intervalence Compounds. *Chem. - Eur. J.* **2000**, *6* (4), 581–588.
- (54) Hush, N. S. Intervalence-Transfer Absorption. Part 2. Theoretical Considerations and Spectroscopic Data. In *Progress in Inorganic Chemistry*; Wiley, 2007.
- (55) Mulliken, R. S. Intensities of Electronic Transitions in Molecular Spectra II. Charge-Transfer Spectra. *J. Chem. Phys.* **1939**, *7* (1), 20–34.
- (56) Cave, R. J.; Newton, M. D. Generalization of the Mulliken-Hush treatment for the calculation of electron transfer matrix elements. *Chem. Phys. Lett.* **1996**, *249* (1), 15–19.
- (57) Oh, D. H.; Sano, M.; Boxer, S. G. Electroabsorption (Stark effect) spectroscopy of mono- and biruthenium charge-transfer complexes: measurements of changes in dipole moments and other electrooptic properties. *J. Am. Chem. Soc.* **1991**, *113* (18), 6880–6890.
- (58) Karki, L.; Hupp, J. T. Orbital Specific Charge Transfer Distances, Solvent Reorganization Energies, and Electronic Coupling Energies: Electronic Stark Effect Studies of Parallel and Orthogonal Intervalence Transfer in (NC)₅OsII-CN-RuIII(NH₃)₅. *J. Am. Chem. Soc.* **1997**, *119* (17), 4070–4073.
- (59) Onuchic, J. N.; Beratan, D. N.; Hopfield, J. J. Some aspects of electron-transfer reaction dynamics. *J. Phys. Chem.* **1986**, *90* (16), 3707–3721.
- (60) Newton, M. D.; Sutin, N. Electron Transfer Reactions in Condensed Phases. *Annu. Rev. Phys. Chem.* **1984**, *35* (1), 437–480.
- (61) Newton, M. D. Electronic coupling in electron transfer and the influence of nuclear modes: theoretical and computational probes. *Theor. Chem. Acc.* **2003**, *110* (5), 307–321.
- (62) Butler, L. J. Chemical Reaction Dynamics Beyond the Born-Oppenheimer Approximation. *Annu. Rev. Phys. Chem.* **1998**, *49* (1), 125–171.
- (63) Sumi, H. Adiabatic versus Non-Adiabatic Electron Transfer. In *Electron Transfer in Chemistry*; Balzani, V., Ed.; Wiley, 2001; pp 64–108. DOI: [10.1002/9783527618248](https://doi.org/10.1002/9783527618248)
- (64) Delor, M.; Sazanovich, I. V.; Towrie, M.; Weinstein, J. A. Probing and Exploiting the Interplay between Nuclear and Electronic Motion in Charge Transfer Processes. *Acc. Chem. Res.* **2015**, *48* (4), 1131–1139.
- (65) Schäfer, J.; Holzapfel, M.; Mladenova, B.; Kattnig, D.; Krummenacher, I.; Braunschweig, H.; Grampp, G.; Lambert, C. Hole Transfer Processes in meta- and para-Conjugated Mixed Valence Compounds: Unforeseen Effects of Bridge Substituents and Solvent Dynamics. *J. Am. Chem. Soc.* **2017**, *139* (17), 6200–6209.
- (66) Sparpaglione, M.; Mukamel, S. Adiabatic vs. nonadiabatic electron transfer and longitudinal solvent dielectric relaxation: beyond the Debye model. *J. Phys. Chem.* **1987**, *91* (15), 3938–3943.
- (67) Frauenfelder, H.; Wolynes, P. Rate theories and puzzles of hemeprotein kinetics. *Science* **1985**, *229* (4711), 337–345.
- (68) Zener, C.; Fowler, R. H. Non-adiabatic crossing of energy levels. *Proc. R. Soc. London, Ser. A* **1932**, *137* (833), 696–702.
- (69) A Theory of Energy Transfer on Collisions. In *Collected Papers of L.D. Landau*; Ter Haar, D., Ed.; Pergamon, 1965; Chapter 7, pp 52–59.
- (70) A Theory of Energy Transfer. II. In *Collected Papers of L.D. Landau*; Ter Haar, D., Ed.; Pergamon, 1965; Chapter 9, pp 63–66.
- (71) Newton, M. D. Quantum chemical probes of electron-transfer kinetics: the nature of donor-acceptor interactions. *Chem. Rev.* **1991**, *91* (5), 767–792.
- (72) Creutz, C. Nonadiabatic, Short-Range, Intramolecular Electron Transfer from Ruthenium(II) to Cobalt(III) Complexes. *J. Phys. Chem. B* **2007**, *111* (24), 6713–6717.
- (73) Sutin, N. Theory of Electron Transfer Reactions: Insights and Hindsights. In *Progress in Inorganic Chemistry*; Wiley, 1983.
- (74) Weaver, M. J. Dynamical solvent effects on activated electron-transfer reactions: principles, pitfalls, and progress. *Chem. Rev.* **1992**, *92* (3), 463–480.
- (75) Maroncelli, M.; MacInnis, J.; Fleming, G. R. Polar Solvent Dynamics and Electron-Transfer Reactions. *Science* **1989**, *243* (4899), 1674–1681.
- (76) Silverman, J.; Dodson, R. W. The Exchange Reaction between the Two Oxidation States of Iron in Acid Solution. *J. Phys. Chem.* **1952**, *56* (7), 846–852.
- (77) Braddock, J. N.; Meyer, T. J. Kinetics of the oxidation of hexaaquoiron(2+) by polypyridine complexes of ruthenium(III). Negative enthalpies of activation. *J. Am. Chem. Soc.* **1973**, *95* (10), 3158–3162.
- (78) Jarzęcki, A. A.; Anbar, A. D.; Spiro, T. G. DFT Analysis of Fe(H₂O)₆³⁺ and Fe(H₂O)₆²⁺ Structure and Vibrations; Implications for Isotope Fractionation. *J. Phys. Chem. A* **2004**, *108* (14), 2726–2732.
- (79) Brunschwig, B. S.; Creutz, C.; Macartney, D. H.; Sham, T. K.; Sutin, N. The role of inner-sphere configuration changes in electron-exchange reactions of metal complexes. *Faraday Discuss. Chem. Soc.* **1982**, *74* (0), 113–127.
- (80) Hair, N. J.; Beattie, J. K. Structure of hexaaquairon(III) nitrate trihydrate. Comparison of iron(II) and iron(III) bond lengths in high-spin octahedral environments. *Inorg. Chem.* **1977**, *16* (2), 245–250.
- (81) Sutin, N. Theory of Electron Transfer Reactions: Insights and Hindsights. In *Progress in Inorganic Chemistry*. In *Progress in Inorganic Chemistry*; Lippard, S. J., Ed.; Wiley, 2007.
- (82) Newton, M. D. Formalisms for electron-exchange kinetics in aqueous solution and the role of Ab initio techniques in their implementation. *Int. J. Quantum Chem.* **1980**, *18* (S14), 363–391.
- (83) Brunschwig, B. S.; Logan, J.; Newton, M. D.; Sutin, N. A semiclassical treatment of electron-exchange reactions. Application to the hexaaquoiron(II)-hexaaquoiron(III) system. *J. Am. Chem. Soc.* **1980**, *102* (18), 5798–5809.
- (84) Hush, N. S. Parameters of Electron-Transfer Kinetics. In *Mechanistic Aspects of Inorganic Reactions*; American Chemical Society: Washington, DC, 1982; Vol. 198, pp 301–332.
- (85) Sutin, N.; Brunschwig, B. S. Electron Transfer in Weakly Interacting Systems. In *Mechanistic Aspects of Inorganic Reactions*; American Chemical Society: Washington, DC, 1982; Vol. 198, pp 105–135.
- (86) Steinfeld, J. I.; Francisco, J. S.; Hase, W. L. *Chemical Kinetics and Dynamics*, 2nd ed.; Prentice Hall: NJ, 1998.
- (87) Kavarnos, G. J.; Turro, N. J. Photosensitization by reversible electron transfer: theories, experimental evidence, and examples. *Chem. Rev.* **1986**, *86* (2), 401–449.
- (88) Biner, M.; Buergi, H. B.; Ludi, A.; Roehr, C. Crystal and molecular structures of [Ru(bpy)₃](PF₆)₃ and [Ru(bpy)₃](PF₆)₂ at 105 K. *J. Am. Chem. Soc.* **1992**, *114* (13), 5197–5203.
- (89) Marcus, Y. Ionic radii in aqueous solutions. *Chem. Rev.* **1988**, *88* (8), 1475–1498.
- (90) Powers, M. J.; Meyer, T. J. Intervalence transfer in the mixed-valence ion [(bpy)₂(py)Ru(4,4'-bpy)Ru(py)(bpy)₂]S⁺. *Inorg. Chem.* **1978**, *17* (7), 1785–1790.
- (91) Sutton, J. E.; Taube, H. Metal to metal interactions in weakly coupled mixed-valence complexes based on ruthenium ammines. *Inorg. Chem.* **1981**, *20* (10), 3125–3134.
- (92) Young, R. C.; Keene, F. R.; Meyer, T. J. Measurement of rates of electron transfer between tris(2,2'-bipyridine)ruthenium(3+) and tris(1,10-phenanthroline)iron(2+) ions and between tris(1,10-phenanthroline)ruthenium(3+) and tris(2,2'-bipyridine)ruthenium(2+) ions by differential excitation flash photolysis. *J. Am. Chem. Soc.* **1977**, *99* (8), 2468–2473.
- (93) Siders, P.; Marcus, R. A. Quantum effects in electron-transfer reactions. *J. Am. Chem. Soc.* **1981**, *103* (4), 741–747.
- (94) Marcus, R. A. Electron transfer reactions in chemistry theory and experiment. *J. Electroanal. Chem.* **1997**, *438* (1), 251–259.
- (95) Roth, J. P.; Yoder, J. C.; Won, T.-J.; Mayer, J. M. Application of the Marcus Cross Relation to Hydrogen Atom Transfer Reactions. *Science* **2001**, *294* (5551), 2524–2526.

- (96) Ratner, M. A.; Levine, R. D. A thermodynamic derivation of the cross-relations for rates of electron-transfer reactions. *J. Am. Chem. Soc.* **1980**, *102* (15), 4898–4900.
- (97) Albery, W. J. The Application of the Marcus Relation to Reactions in Solution. *Annu. Rev. Phys. Chem.* **1980**, *31* (1), 227–263.
- (98) Lin, C. T.; Boettcher, W.; Chou, M.; Creutz, C.; Sutin, N. Mechanism of the quenching of the emission of substituted polypyridineruthenium(II) complexes by iron(III), chromium(III), and europium(III) ions. *J. Am. Chem. Soc.* **1976**, *98* (21), 6536–6544.
- (99) Marcus, R. A. On the Theory of Electron-Transfer Reactions. VI. Unified Treatment for Homogeneous and Electrode Reactions. *J. Chem. Phys.* **1965**, *43* (2), 679–701.
- (100) Mayer, J. M. Simple Marcus-Theory-Type Model for Hydrogen-Atom Transfer/Proton-Coupled Electron Transfer. *J. Phys. Chem. Lett.* **2011**, *2* (12), 1481–1489.
- (101) Hupp, J. T.; Weaver, M. J. Prediction of electron-transfer reactivities from contemporary theory: unified comparisons for electrochemical and homogeneous reactions. *J. Phys. Chem.* **1985**, *89* (13), 2795–2804.
- (102) Rehm, D.; Weller, A. Kinetics of Fluorescence Quenching by Electron and H-Atom Transfer. *Isr. J. Chem.* **1970**, *8* (2), 259–271.
- (103) Farid, S.; Dinnocenzo, J. P.; Merkel, P. B.; Young, R. H.; Shukla, D.; Guirado, G. Reexamination of the Rehm-Weller Data Set Reveals Electron Transfer Quenching That Follows a Sandros-Boltzmann Dependence on Free Energy. *J. Am. Chem. Soc.* **2011**, *133* (30), 11580–11587.
- (104) Rosspeintner, A.; Kattnig, D. R.; Angulo, G.; Landgraf, S.; Gramp, G. The Rehm-Weller Experiment in View of Distant Electron Transfer. *Chem. - Eur. J.* **2008**, *14* (20), 6213–6221.
- (105) Kikuchi, K.; Takahashi, Y.; Katagiri, T.; Niwa, T.; Hoshi, M.; Miyashi, T. A critical consideration on the lack of inverted region in the Rehm—Weller plot for electron-transfer fluorescence quenching. *Chem. Phys. Lett.* **1991**, *180* (5), 403–408.
- (106) Rosspeintner, A.; Angulo, G.; Vauthey, E. Bimolecular Photoinduced Electron Transfer Beyond the Diffusion Limit: The Rehm-Weller Experiment Revisited with Femtosecond Time Resolution. *J. Am. Chem. Soc.* **2014**, *136* (5), 2026–2032.
- (107) Closs, G. L.; Miller, J. R. Intramolecular Long-Distance Electron Transfer in Organic Molecules. *Science* **1988**, *240* (4851), 440–447.
- (108) Jortner, J. Temperature dependent activation energy for electron transfer between biological molecules. *J. Chem. Phys.* **1976**, *64* (12), 4860–4867.
- (109) Fox, L. S.; Kozik, M.; Winkler, J. R.; Gray, H. B. Gaussian Free-Energy Dependence of Electron-Transfer Rates in Iridium Complexes. *Science* **1990**, *247* (4946), 1069–1071.
- (110) Davis, W. B.; Ratner, M. A.; Wasielewski, M. R. Conformational Gating of Long Distance Electron Transfer through Wire-like Bridges in Donor-Bridge-Acceptor Molecules. *J. Am. Chem. Soc.* **2001**, *123* (32), 7877–7886.
- (111) Weiss, E. A.; Tauber, M. J.; Kelley, R. F.; Ahrens, M. J.; Ratner, M. A.; Wasielewski, M. R. Conformationally Gated Switching between Superexchange and Hopping within Oligo-p-phenylene-Based Molecular Wires. *J. Am. Chem. Soc.* **2005**, *127* (33), 11842–11850.
- (112) Spettel, K. E.; Damrauer, N. H. Exploiting Conformational Dynamics of Structurally Tuned Aryl-Substituted Terpyridyl Ruthenium(II) Complexes to Inhibit Charge Recombination in Dye-Sensitized Solar Cells. *J. Phys. Chem. C* **2016**, *120* (20), 10815–10829.
- (113) Benniston, A. C.; Harriman, A.; Li, P.; Sams, C. A.; Ward, M. D. Orientational Control of Electronic Coupling in Mixed-Valence, Binuclear Ruthenium(II)-Bis(2,2':6,2"-Terpyridine) Complexes. *J. Am. Chem. Soc.* **2004**, *126* (42), 13630–13631.
- (114) Solomon, E. I.; Lowery, M. D.; Guckert, J. A.; LaCroix, L. B. Electron Transfer in Bioinorganic Chemistry. In *Electron Transfer Reactions*; American Chemical Society: Washington, DC, 1997; Vol. 253, pp 317–330.
- (115) Vallee, B. L.; Williams, R. J. Metalloenzymes: the entatic nature of their active sites. *Proc. Natl. Acad. Sci. U. S. A.* **1968**, *59* (2), 498–505.
- (116) Kuss-Petermann, M.; Wenger, O. S. Electron Transfer Rate Maxima at Large Donor-Acceptor Distances. *J. Am. Chem. Soc.* **2016**, *138* (4), 1349–1358.
- (117) Closs, G. L.; Calcaterra, L. T.; Green, N. J.; Penfield, K. W.; Miller, J. R. Distance, stereoelectronic effects, and the Marcus inverted region in intramolecular electron transfer in organic radical anions. *J. Phys. Chem.* **1986**, *90* (16), 3673–3683.
- (118) Helms, A.; Heiler, D.; McLendon, G. Dependence of electron transfer rates on donor-acceptor angle in bis-porphyrin adducts. *J. Am. Chem. Soc.* **1991**, *113* (11), 4325–4327.
- (119) Moser, C. C.; Keske, J. M.; Warncke, K.; Farid, R. S.; Dutton, P. L. Nature of biological electron transfer. *Nature* **1992**, *355* (6363), 796–802.
- (120) Gray, H. B.; Winkler, J. R. Long-range electron transfer. *Proc. Natl. Acad. Sci. U. S. A.* **2005**, *102* (10), 3534–3539.
- (121) Tavernier, H. L.; Fayer, M. D. Distance Dependence of Electron Transfer in DNA: The Role of the Reorganization Energy and Free Energy. *J. Phys. Chem. B* **2000**, *104* (48), 11541–11550.
- (122) Beratan, D.; Betts, J.; Onuchic, J. Protein electron transfer rates set by the bridging secondary and tertiary structure. *Science* **1991**, *252* (5010), 1285–1288.
- (123) Lewis, F. D.; Wu, T.; Zhang, Y.; Letsinger, R. L.; Greenfield, S. R.; Wasielewski, M. R. Distance-Dependent Electron Transfer in DNA Hairpins. *Science* **1997**, *277* (5326), 673–676.
- (124) Devault, D. Quantum mechanical tunnelling in biological systems. *Q. Rev. Biophys.* **1980**, *13* (4), 387–564.
- (125) Helms, A.; Heiler, D.; McLendon, G. Electron transfer in bis-porphyrin donor-acceptor compounds with polyphenylene spacers shows a weak distance dependence. *J. Am. Chem. Soc.* **1992**, *114* (15), 6227–6238.
- (126) Wiberg, J.; Guo, L.; Pettersson, K.; Nilsson, D.; Ljungdahl, T.; Mårtensson, J.; Albinsson, B. Charge Recombination versus Charge Separation in Donor-Bridge-Acceptor Systems. *J. Am. Chem. Soc.* **2007**, *129* (1), 155–163.
- (127) Wenger, O. S.; Leigh, B. S.; Villahermosa, R. M.; Gray, H. B.; Winkler, J. R. Electron Tunneling Through Organic Molecules in Frozen Glasses. *Science* **2005**, *307* (5706), 99–102.
- (128) Wenger, O. S. How Donor-Bridge-Acceptor Energetics Influence Electron Tunneling Dynamics and Their Distance Dependencies. *Acc. Chem. Res.* **2011**, *44* (1), 25–35.
- (129) Davis, W. B.; Svec, W. A.; Ratner, M. A.; Wasielewski, M. R. Molecular-wire behaviour in p-phenylenevinylene oligomers. *Nature* **1998**, *396* (6706), 60–63.
- (130) Yonemoto, E. H.; Riley, R. L.; Kim, Y. I.; Atherton, S. J.; Schmehl, R. H.; Mallouk, T. E. Photoinduced electron transfer in covalently linked ruthenium tris(bipyridyl)-viologen molecules: observation of back electron transfer in the Marcus inverted region. *J. Am. Chem. Soc.* **1992**, *114* (21), 8081–8087.
- (131) Yonemoto, E. H.; Riley, R. L.; Kim, Y. I.; Atherton, S. J.; Schmehl, R. H.; Mallouk, T. E. Photoinduced electron transfer in covalently linked ruthenium tris(bipyridyl)-viologen molecules: observation of back electron transfer in the Marcus inverted region. [Erratum to document cited in CA117(18):18372S]. *J. Am. Chem. Soc.* **1993**, *115* (12), 5348–5348.
- (132) Yonemoto, E. H.; Saupe, G. B.; Schmehl, R. H.; Hubig, S. M.; Riley, R. L.; Iverson, B. L.; Mallouk, T. E. Electron-Transfer Reactions of Ruthenium Trisbipyridyl-Viologen Donor-Acceptor Molecules: Comparison of the Distance Dependence of Electron Transfer-Rates in the Normal and Marcus Inverted Regions. *J. Am. Chem. Soc.* **1994**, *116* (11), 4786–4795.
- (133) Kuss-Petermann, M.; Wenger, O. S. Increasing Electron-Transfer Rates with Increasing Donor-Acceptor Distance. *Angew. Chem., Int. Ed.* **2016**, *55* (2), 815–819.
- (134) Kuss-Petermann, M.; Wenger, O. S. Unusual distance dependences of electron transfer rates. *Phys. Chem. Chem. Phys.* **2016**, *18* (28), 18657–18664.

- (135) Hanss, D.; Wenger, O. S. Tunneling Barrier Effects on Photoinduced Charge Transfer through Covalent Rigid Rod-Like Bridges. *Inorg. Chem.* **2009**, *48* (2), 671–680.
- (136) Indelli, M. T.; Chiorboli, C.; Flamigni, L.; De Cola, L.; Scandola, F. Photoinduced Electron Transfer across Oligo-p-phenylene Bridges. Distance and Conformational Effects in Ru(II)-Rh(III) Dyads. *Inorg. Chem.* **2007**, *46* (14), 5630–5641.
- (137) Brunschwig, B. S.; Ehrenson, S.; Sutin, N. The distance dependence of electron transfer reactions: rate maxima and rapid rates at large reactant separations. *J. Am. Chem. Soc.* **1984**, *106* (22), 6858–6859.
- (138) Neumann, S.; Wenger, O. S. Fundamentally Different Distance Dependences of Electron-Transfer Rates for Low and High Driving Forces. *Inorg. Chem.* **2019**, *58* (1), 855–860.
- (139) Hush, N. S. Homogeneous and heterogeneous optical and thermal electron transfer. *Electrochim. Acta* **1968**, *13* (5), 1005–1023.
- (140) Creutz, C.; Taube, H. Direct approach to measuring the Franck-Condon barrier to electron transfer between metal ions. *J. Am. Chem. Soc.* **1969**, *91* (14), 3988–3989.
- (141) Zhang, L. T.; Ko, J.; Ondrechen, M. J. Electronic structure of the Creutz-Taube ion. *J. Am. Chem. Soc.* **1987**, *109* (6), 1666–1671.
- (142) Fuerholz, U.; Buergi, H. B.; Wagner, F. E.; Stebler, A.; Ammeter, J. H.; Krausz, E.; Clark, R. J. H.; Stead, M. J.; Ludi, A. The Creutz-Taube complex revisited. *J. Am. Chem. Soc.* **1984**, *106* (1), 121–123.
- (143) Lu, H.; Petrov, V.; Hupp, J. T. Intervalence excitation of the Creutz-Taube ion. Resonance Raman and time-dependent scattering studies of Franck-Condon effects. *Chem. Phys. Lett.* **1995**, *235* (5), 521–527.
- (144) De la Rosa, R.; Chang, P. J.; Salaymeh, F.; Curtis, J. C. Redox asymmetry and metal-metal coupling in pyrazine-bridged ruthenium dimers. *Inorg. Chem.* **1985**, *24* (25), 4229–4231.
- (145) D'Alessandro, D. M.; Keene, F. R. A cautionary warning on the use of electrochemical measurements to calculate comproportionation constants for mixed-valence compounds. *Dalton Trans.* **2004**, *23*, 3950–3954.
- (146) Ernst, S.; Kasack, V.; Kaim, W. What determines the comproportionation constant in molecule-bridged mixed-valence complexes? Evidence for the crucial role of the ligand LUMO in four ruthenium(II)ruthenium(III) dimers. *Inorg. Chem.* **1988**, *27* (7), 1146–1148.
- (147) D'Alessandro, D. M.; Keene, F. R. Current trends and future challenges in the experimental, theoretical and computational analysis of intervalence charge transfer (IVCT) transitions. *Chem. Soc. Rev.* **2006**, *35* (5), 424–440.
- (148) Ito, T.; Hamaguchi, T.; Nagino, H.; Yamaguchi, T.; Washington, J.; Kubiak, C. P. Effects of Rapid Intramolecular Electron Transfer on Vibrational Spectra. *Science* **1997**, *277* (5326), 660–663.
- (149) Lonergan, C. H.; Salsman, J. C.; Ronco, S.; Dolkas, L. M.; Kubiak, C. P. Solvent Dynamical Control of Electron-Transfer Rates in Mixed-Valence Complexes Observed by Infrared Spectral Line Shape Coalescence. *J. Am. Chem. Soc.* **2002**, *124* (22), 6236–6237.
- (150) Kubiak, C. P. Inorganic Electron Transfer: Sharpening a Fuzzy Border in Mixed Valency and Extending Mixed Valency across Supramolecular Systems. *Inorg. Chem.* **2013**, *52* (10), 5663–5676.
- (151) Glover, S. D.; Goeltz, J. C.; Lear, B. J.; Kubiak, C. P. Inter- or intramolecular electron transfer between triruthenium clusters: we'll cross that bridge when we come to it. *Coord. Chem. Rev.* **2010**, *254* (3), 331–345.
- (152) Ito, T.; Hamaguchi, T.; Nagino, H.; Yamaguchi, T.; Kido, H.; Zavarine, I. S.; Richmond, T.; Washington, J.; Kubiak, C. P. Electron Transfer on the Infrared Vibrational Time Scale in the Mixed Valence State of 1,4-Pyrazine- and 4,4'-Bipyridine-Bridged Ruthenium Cluster Complexes. *J. Am. Chem. Soc.* **1999**, *121* (19), 4625–4632.
- (153) Goeltz, J. C.; Benson, E. E.; Kubiak, C. P. Electronic Structural Effects in Self-Exchange Reactions. *J. Phys. Chem. B* **2010**, *114* (45), 14729–14734.
- (154) Luo, Y.; Tran, J. H.; Wächtler, M.; Schulz, M.; Barthelmes, K.; Winter, A.; Rau, S.; Schubert, U. S.; Dietzek, B. Remote control of electronic coupling - modification of excited-state electron-transfer rates in Ru(tpy)₂-based donor-acceptor systems by remote ligand design. *Chem. Commun.* **2019**, *55* (16), 2273–2276.
- (155) Piechota, E. J.; Troian-Gautier, L.; Sampaio, R. N.; Brennaman, M. K.; Hu, K.; Berlinguette, C. P.; Meyer, G. J. Optical Intramolecular Electron Transfer in Opposite Directions through the Same Bridge That Follows Different Pathways. *J. Am. Chem. Soc.* **2018**, *140* (23), 7176–7186.
- (156) Sampaio, R. N.; Piechota, E. J.; Troian-Gautier, L.; Maurer, A. B.; Hu, K.; Schauer, P. A.; Blair, A. D.; Berlinguette, C. P.; Meyer, G. J. Kinetics teach that electronic coupling lowers the free-energy change that accompanies electron transfer. *Proc. Natl. Acad. Sci. U. S. A.* **2018**, *115* (28), 7248–7253.
- (157) Piechota, E. J.; Sampaio, R. N.; Troian-Gautier, L.; Maurer, A. B.; Berlinguette, C. P.; Meyer, G. J. Entropic Barriers Determine Adiabatic Electron Transfer Equilibrium. *J. Phys. Chem. C* **2019**, *123* (6), 3416–3425.